Article:

Magnall, JM, Gleeson, SA, Poulton, SW orcid.org/0000-0001-7621-189X et al. (2 more authors) (2018) Links between seawater paleoredox and the formation of sediment-hosted massive sulphide (SHMS) deposits — Fe speciation and Mo isotope constraints from Late Devonian mudstones. Chemical Geology, 490. pp. 45-60. ISSN 0009-2541

https://doi.org/10.1016/j.chemgeo.2018.05.005

Links between seawater paleoredox and the formation of sediment-hosted massive sulphide (SHMS) deposits – Fe speciation and Mo isotope constraints from Late Devonian mudstones

Joseph M. Magnall[1], Sarah A. Gleeson[1,2], Simon W. Poulton[3], Gwyneth G. Gordon[4], and Suzanne Paradis[5]

[1] GFZ German Research Centre for Geosciences, 14473 Potsdam, Germany
[2] Institute of Geological Sciences, Freie Universität Berlin, Malteserstrasse, 74-100, Berlin, 12249, Germany
[3] School of Earth and Environment, University of Leeds, Leeds, LS2 9JT, UK
[4] School of Earth and Space Exploration, Arizona State University, Tempe, AZ 85287, United States
[5] Geological Survey of Canada, Box 6000, 9860 West Saanich Road, Sidney, British Columbia, V8L 4B2, Canada

ABSTRACT

Many models of sediment hosted massive sulphide (SHMS) deposit formation invoke basin restriction events that resulted in long-term stagnation and anoxia, in which sulphidic (euxinic) conditions ultimately prevailed. Euxinic conditions are then thought to provide a chemical trap for hydrothermally exhaled base metals. Here, we present Fe speciation and Mo isotope data for organic-rich mudstones from two drill-holes intersecting Upper Devonian strata, deposited along the passive margin of ancestral North America. One drill-hole intersects a 35 m thick sequence of SHMS mineralisation, while the other intersects correlative, un-mineralised strata. All samples have high Fe_{HR}/Fe_T values (>0.38), indicating water-column anoxia. For the majority of samples in the un-mineralised drill-hole, the levels of pyritisation fall below the threshold typically used to define euxinic conditions ($Fe_{PY}/Fe_{HR} \leq 0.7$). In contrast, higher levels of pyritisation in the mineralised drill-hole (median Fe_{PY}/Fe_{HR} = 0.86) likely developed via diagenetic pyrite enrichment. Whereas Pb and Zn are negatively correlated with Mo, Mo-U co-variation is consistent with Fe (oxyhydr)oxide particulate shuttling in the water-column. In addition, a weak correlation between TOC/P and Mo provides further evidence that Mo was sourced via authigenic, rather than hydrothermal, processes. The δ^{98}Mo values (+0.35 to +0.71‰) are uniform between both drill-holes, and substantially lower than constraints for Late Devonian seawater (+1.5 to +2.0‰), consistent with Mo adsorption to Fe (oxyhydr)oxides. Collectively, the data provide evidence that local seawater was dominantly ferruginous (anoxic, non-sulphidic) at Macmillan Pass. Regional variability in the extent of ferruginous (low TOC/P) and euxinic (high TOC/P) conditions likely contributed to a balance between P regeneration and P enrichment that maintained nutrient availability and productivity in the Selwyn Basin during the Late Devonian. We argue that high primary productivity and enhanced organic carbon burial are key variables for promoting sulphate reduction in the sub-surface. Moreover, how such conditions are maintained over long periods of basin evolution is more important for producing effective metal traps in SHMS systems, rather than a specific, localised redox condition of seawater (i.e. euxinia).

INTRODUCTION

Sediment-hosted massive sulphide (SHMS) deposits represent the anomalous enrichment of reduced sulphur and base metals (Pb, Zn, Fe) within organic-rich marine strata (Ohmoto and Goldhaber, 1997). A major challenge for previous studies on SHMS deposits has been to determine the nature of the relationship between ambient paleoredox conditions and mineralisation. Many deposits contain bedded (stratiform) sulphide mineralisation, which has led to the development of sedimentary exhalative (SEDEX) models involving sulphide precipitation from a stagnant water-column, where anoxic, sulphidic conditions (dissolved $H_2S > Fe^{2+}$; euxinic) develop in restricted marine sub-basins (Goodfellow et al., 1993). Indeed, the development of euxinic conditions has been proposed as the chemical trap for hydrothermally exhaled base metals, and also provides a key component in the explanation for the secular distribution of SHMS deposits within the geologic record (Goodfellow, 1987; Lyons et al., 2006; Turner, 1992).

Ultimately, this euxinic basin paradigm forms a framework for how basin architecture (i.e. restriction) and geochemistry (i.e. stagnation, euxinia) is interpreted in SHMS systems, which informs exploration models and the targeting of new discoveries.

Combining the iron and Mo based redox proxies can provide an important framework for evaluating seawater paleoredox across different scales, both local and global (Scott and Lyons, 2012). Molybdenum is the most abundant transition metal in seawater, and is homogenously distributed within the modern oceans (~8 x 10^5 yr residence time; Emerson and Huested, 1991). Importantly, adsorption of Mo to Fe-Mn (oxyhydr)oxides in oxic seawater results in a large isotopic fractionation, leading to modern seawater with a high δ^{98}Mo value (+2.4‰; Barling et al., 2001; Barling and Anbar, 2004; Poulson et al., 2006; Siebert et al., 2003). In contrast, there is minimal isotopic fractionation between seawater and sediments deposited under strongly euxinic conditions in which H_2S concentrations exceed 11 µM (Erickson and Helz, 2000; Nägler et al., 2005; Neubert et al., 2008). Assuming invariant Mo input to the oceans, periods of Earth history with expanded euxinia are therefore characterised by δ^{98}Mo values that are lower relative to modern oceans (e.g. Arnold et al., 2004). However, accurate interpretations require independent constraints of local depositional redox conditions, and the need to specifically demonstrate the occurrence of strongly euxinic conditions in which no fractionation occurs between seawater and sediment (e.g. Gordon et al., 2009). This is typically achieved by the combined interpretation of Mo and Fe geochemistry (Scott and Lyons, 2012), with the latter involving an evaluation of sediment Fe enrichments and the degree to which Fe occurs within pyrite relative to other phases containing reactive Fe (e.g. carbonate and oxide phases; Poulton and Canfield, 2005).

Despite the proposed link between seawater paleoredox and sulphide mineralisation, a combined approach using Mo and Fe geochemistry has not yet been attempted on the organic-rich mudstones that host SHMS deposits. In this study, we focus on Upper Devonian organic-rich mudstones from the Selwyn Basin which, like other sedimentary basins of this age, is host to fine-grained siliciclastic rocks deposited along the continental margin of ancestral North America

(Fig. 1). Unlike other Late Devonian basins of North America, the Selwyn Basin also hosts SHMS mineralisation (Fig. 2A, B). At Macmillan Pass, two SHMS deposits occur within Frasnian strata (Fig. 2C), where the full deposit architectures are well-preserved, comprising a discrete feeder zone of massive sulphide and iron carbonate mineralisation overlain by a laterally extensive sequence (hundreds of meters) of bedded sulphide and barite mineralization (between ~5 and 40 meters thick). This provides an opportunity to address a number of questions relating to seawater paleoredox during the Late Devonian and possible relationships with SHMS mineralisation, including: (1) is there any evidence of a hydrothermal Mo flux at Macmillan Pass, and if so, what is the isotopic composition? 2) How does the Selwyn Basin compare in terms of paleoredox to other sedimentary basins hosting organic rich mudstones? 3) Is there a clear genetic relationship between seawater paleoredox and sulphide mineralisation?

METHODS

Samples

Samples were collected from three correlated drill-holes (76-17, TYK-5 and TYK-1; Fig. 2C and 3), including 37 samples of un-mineralised mudstones and five samples from the mineralised hydrothermal vent at the Tom deposit (Fig. 4). The stockwork veining in the vent complex occurs immediately beneath the bedded mineralisation (see TYK-1 in Fig. 3 and Fig. 4), and represents the main conduit of hydrothermal upflow in the SHMS systems at Macmillan Pass (Magnall et al. 2016a).

Hand specimens of the un-mineralised mudstones were examined under a binocular microscope to identify small-scale sedimentological features, and sub-samples were cut parallel to bedding for geochemical analysis, minimising the vertical stratigraphic thickness of the sample (< 2cm; Fig. 4). Care was taken to collect only the most homogenous, fine-grained samples, and those containing high concentrations of euhedral pyrite, obvious detrital input (e.g. silt beds), and any evidence of alteration (veining; hydrothermal or tectonic) were avoided. The vent complex samples preserve an assemblage of ankerite veining and massive sulphide mineralisation within variably altered organic-rich mudstone. The hydrothermal fluid entering the vent complex was hot (> 250 °C) and reducing ($fO_2 = 10^{-35}$) but rapidly cooled upon mixing with diagenetic fluids (Magnall et al., 2016a).

Chemical analyses

Bulk rock powders for all samples (un-mineralised mudstones and mineralised vent samples) were analysed for trace elements by aqua-regia digestion and ICP-MS at ACME laboratories (Vancouver, Canada). Data quality and accuracy were monitored through the analysis of in-house laboratory quartz blanks and internal standards, and the insertion of blind quartz blanks and certified reference materials with the unknowns. As the un-mineralised mudstones and mineralised vent complex samples have substantially different matrixes, different reference materials were used; the SBC-1 and SGR-1b (USGS standards) were used for the mudstones whereas OREAS standards (131a and 134a) were used for the mineralised vent complex samples. The measured concentrations of the reference materials were always within the certified range.

For the un-mineralised mudstones, the sequential extraction technique of Poulton and Canfield (2005) was used to quantify highly reactive Fe (Fe_{HR}), which represents Fe incorporated into pyrite (Fe_{PY}), carbonates (e.g. ankerite, siderite; Fe_{CARB}), ferric oxides (goethite, hematite; Fe_{OX}), and magnetite (Fe_{MAG}). This involved the sequential extraction of Fe_{CARB} by a sodium acetate leach (48 h at 50°C), Fe_{OX} by sodium dithionite leach (2 h at room temperature) and Fe_{MAG} by ammonium oxalate leach (6 h at room temperature). Atomic absorption spectroscopy (AAS) was then used to quantify the Fe in each sequential extraction. The Fe_{PY} fraction was calculated from the extraction of sulphide as Ag_2S following a hot chromous chloride distillation (Canfield et al., 1986). The relative standard deviation of repeat analyses of Fe_{PY} was 14% (n = 6), and for all other extractions < 8% (n = 13).

Isotopic analyses

Molybdenum isotope analyses were performed at the W.M. Keck Foundation Laboratory for Environmental Biogeochemistry (Arizona State University) on a Thermo Finnigan Neptune MC-ICP-MS with an Elemental Scientific Apex-Q and a PFA nebuliser. Splits of the same bulk rock powders of un-mineralised mudstone were ashed at 550°C overnight to degrade organic matter. Aliquots of 100 mg were sonicated in a combination of trace-metal-grade nitric and hydrofluoric acids, then heated in sealed Teflon vessels at 120°C overnight. This was followed by nitric and hydrochloric acids if digestion was not complete. Acids were evaporated off under HEPA filtered air, and samples were re-dissolved in 6 M trace metal grade hydrochloric acid. Samples were purified using a two-column method previously reported (Duan et al., 2010). In brief, Biorad AG1X-8 anion resin is used to separate Fe and Mo from the resin; the matrix is eluted in 6M HCl, and the Fe and Mo are co-eluted in 1 M HCl. Biorad AG50WX-8 cation exchange resin is used to sequester Fe in 0.5 M HCl, and elute Mo. To correct for instrumental mass bias and isobaric interferences, samples were doubled-spiked with a calibrated ^{97}Mo–^{100}Mo spike. The following isotopes were measured for 4.1 seconds at 100 cycles per analysis: ^{91}Zr, ^{92}Mo, ^{94}Mo, ^{95}Mo, ^{96}Mo, ^{97}Mo, ^{98}Mo, ^{99}Ru and ^{100}Mo. All Mo isotopes were corrected for mass bias and isobaric interferences with Zr (^{92}Zr, ^{94}Zr and ^{96}Zr).

Sample measurements were bracketed (every two analyses) by an in house standard, RochMo2 (Johnson Matthey Chemical, Specpure ICP-MS standard, Stock #35758, Lot #802309E). Every 10 samples four additional secondary standards were analysed, including NIST SRM3134 (Goldberg et al. 2013), KyotoMo (In-house ICP standard, Kyoto University), ImperialMo (in-house ICP standard, Imperial University) and SDO-1 (USGS rock reference material). The Mo isotope data are presented as delta (δ) values as the parts per thousand (‰) deviation in ^{98}Mo/^{95}Mo relative to the standard:

$$\delta^{98}\mathrm{Mo}\ (‰) = \{[(^{98}\mathrm{Mo}/^{95}\mathrm{Mo})_{\mathrm{sample}} / (^{98}\mathrm{Mo}/^{95}\mathrm{Mo})_{\mathrm{standard}}] -1\} \times 1000$$

The reproducibility of all analysed standard materials compare well with the long-term values. The measured value for NIST SRM 3134 (+0.31‰ ± 0.04, 2σ; n = 12) is slightly higher than the value determined for this reference material (+0.25‰; Goldberg et al., 2013), and 0.06‰ has been subtracted from each sample so that data are reported relative to this interlaboratory scale (Nägler et al., 2014).

RESULTS

The major element chemistry of the un-mineralised mudstones has already been published in Magnall et al. (2015) and is supplemented in Table 1 by trace element data and 5 samples from the vent complex (this study). All chemical (Fe speciation) and Mo isotope data are summarised in Table 2, together with bulk rock $\delta^{34}S$ values reported by Magnall et al. (2016b) that were produced on the same un-mineralised mudstone samples. Down-hole plots of Fe speciation parameters (Fe_{HR}/Fe_T, Fe_{PY}/Fe_{HR}) and Mo geochemistry ($\delta^{98}Mo$, ppm) are presented in Figure 5. Where median values are given in the following text, the interquartile range (Q1 to Q3) is included in parentheses. The un-mineralised mudstones contain high levels of SiO_2 (median 77.0 wt.%; Q1 to Q3 = 72.9 to 80.6). The SiO_2 is largely of biogenic origin (see Magnall et al. 2015), however total Fe (Fe_T) has not been diluted below the concentration considered to give reliable Fe paleo-redox data (Fe_T = 0.5 wt%; Clarkson et al., 2014); samples from drill-hole (DH) 76-17 contain median Fe_T of 1.47 wt.% (Q1 to Q3 = 1.19 to 1.83) and DH-TKY-5 of 2.41 wt.% (Q1 to Q3 = 1.32 to 2.90). Samples from DH-76-17 and DH-TYK-5 preserve contrasting Fe_T/Al ratios, with respective median values of 0.38 (Q1 to Q3 = 0.31 to 0.45) and 0.61 (Q1 to Q3 = 0.29 to 0.67). In samples from DH-TYK-5, Fe_T/Al forms a positive correlation (R^2 = 0.72) with bulk rock $\delta^{34}S$ values (Fig. 6).

In terms of Fe speciation, highly reactive iron (Fe_{HR}), which is a summation of Fe in pyrite (Fe_{PY}), carbonate (Fe_{CARB}), oxide phases (Fe_{OX}) and magnetite (Fe_{MAG}), comprises a major proportion of total Fe (Fe_T) in both drill-holes (Fig. 5). Median Fe_{HR}/Fe_T values are 0.86

(Q1 to Q3 = 0.81 to 0.94) and 0.98 (Q1 to Q3 = 0.95 to 1.02) for samples from 76-17 and TYK-5, respectively. The fraction of Fe_{HR} present as Fe_{PY} is high in both drill-holes (Fig. 5), with median values for Fe_{PY}/Fe_{HR} of 0.72 (Q1 to Q3 = 0.65 to 0.76) in samples from DH-76-17 and 0.85 (Q1 to Q3 = 0.78 to 0.86) for samples from TYK-5. Most of the un-sulphidised Fe_{HR} occurs as Fe_{CARB}, with minor amounts of Fe_{OX} and Fe_{MAG} (see Table 1).

In terms of trace metals (see Fig. 7), the 5 mineralised samples contain high but variable levels of Zn (0.8 wt.%, < 0.1 to 2.5) and Pb (3.8 wt.%, 0.1 to 8.2), but low levels of Mo (3 to 5 ppm). In contrast, the un-mineralised mudstones contain < 100 ppm Pb and mostly < 1000 ppm Zn. Compared to the mineralised vent samples, however, Mo is enriched in the mudstones (18 ppm, Q1 to Q3 = 14 to 21). The mudstone samples have a narrow, normally distributed range of δ^{98}Mo values (0.48‰ ± 0.11), with no systematic relationship between δ^{98}Mo values and Fe_{PY}/Fe_{HR} (Fig. 5). There are weak correlations between Mo and TOC ($r^2 = 0.37$; Fig. 8) and between Mo and TOC/P ($r^2 = 0.43$; Fig. 9a), and a stronger correlation between TOC/P and P/Al ($r^2 = 0.59$; Fig. 9b). Also included in Figures 8 and 9 are recently published data for correlative mudstones from the Richardson Trough (Fraser and Hutchison, 2017), which is a northerly extension of the Selwyn Basin (Figure 1).

DISCUSSION

Iron Geochemistry

The total Fe (Fe_T) budget of marine sediments is comprised of Fe_{HR}, which represents Fe that may undergo redox-controlled mineralogical transformations during diagenesis, together with poorly reactive and unreactive silicate Fe (Raiswell and Canfield, 1998). When normalised to Al (which in most sedimentary environments is immobile), changes in Fe_T/Al typically reflect redox-controlled changes in the Fe_{HR} budget of sediments (Lyons and Severmann, 2006; Scholz et al., 2014). For example, when dissolution of insoluble Fe (oxy)hydroxides occurs in euxinic basins, water column (syngenetic) pyrite formation can result in underlying sediments developing high Fe/Al ratios relative to lithogenic background (Lyons and Severmann, 2006). In contrast, in parts of the modern ocean where both low oxygen and low sulphide concentrations occur, Fe (oxy)hydroxide dissolution in sediment pore fluids results in the release of Fe^{2+} to the water column and the development of relatively low sedimentary Fe/Al ratios (Scholz et al., 2014).

The median Fe/Al value for samples from DH-76-17 (0.38; Fig. 6a) overlaps with correlative mudstones from the Richardson Trough (Fraser and Hutchison, 2017). Combined, the Fe/Al value of samples from the Richardson Trough and DH-76-17 may indicate a regional lithogenic background (e.g. Scholz et al., 2014) that is lower than the upper continental crust value that is commonly used as a reference for shale (0.44; McLennan, 2001). In contrast, the Fe/Al in samples from DH-TYK-5 is higher (median = 0.61), which could indicate Fe_{HR} enrichment associated with syngenetic pyrite formation in a euxinic water column (Lyons and Severmann, 2006). Indeed, there is a good correlation between increasing Fe/Al (Fig. 6b), and more positive bulk rock $\delta^{34}S$ values that are typical of pyrite formation in sulphate limited conditions (Gomes and Hurtgen, 2015). Sulphate limited conditions, however, can occur on different scales; for example, within the water column at a basin scale (Newton et al., 2011) or at a more local scale within diagenetic pore fluids (Borowski et al., 2013). Indeed, recent in situ isotopic analyses of pyrite at Macmillan Pass has established that positive $\delta^{34}S$ values (> 15‰)

developed during diagenesis (i.e. at a local scale), close to the sulphate methane transition zone (SMTZ) (Magnall et al., 2016b). Thus, the trend towards more positive bulk rock $\delta^{34}S$ values at higher Fe/Al in samples from DH-TYK-5 (Fig. 6b) is evidence that Fe enrichment corresponds with a greater proportion of pyrite formed at the SMTZ relative to pyrite formed via bacterial sulphate reduction (BSR). This interpretation is similar to recent work that has documented increasing Fe_{PY}/Fe_{HR} and $\delta^{34}S$ values at the SMTZ along the continental margin of the South China Sea (Lin et al., 2016). In contrast, there is no correlation between Fe/Al and $\delta^{34}S$ in samples from DH-76-17, indicating the predominant generation of pyrite formed during early diagenesis via BSR and there was minimal subsequent Fe enrichment. Nevertheless, in both drill holes (TYK-5 and 76-17) Fe_{HR} still represents the predominant component of Fe_T and greatly exceeds the threshold for deposition under anoxic conditions ($Fe_{HR}/Fe_T > 0.38$; Poulton and Raiswell, 2002; Raiswell and Canfield, 1998).

The degree to which Fe_{HR} is converted to Fe_{PY} can be used to distinguish between anoxic non-sulphidic (ferruginous) and anoxic sulphidic (euxinic) conditions (Poulton and Canfield, 2005). High levels of pyritisation ($Fe_{PY}/Fe_{HR} > 0.7$) suggest a persistently euxinic water-column, whereas lower values ($Fe_{PY}/Fe_{HR} < 0.7$) are more consistent with varying degrees of pyritisation within sulphidic pore fluids (i.e. beneath anoxic, non-sulphidic waters, which are commonly ferruginous) or under weakly or intermittently euxinic conditions (Poulton and Canfield, 2011). Applying this framework to samples from Macmillan Pass is only appropriate for samples from DH-76-17, considering the evidence for diagenetic pyrite enrichment (Fig. 6b). For these samples, a median value for Fe_{PY}/Fe_{HR} of 0.72 represents a high level of pyritisation that does not strongly distinguish between euxinic or ferruginous conditions. Indeed, ferruginous settings that are prone to intermittent euxinia result in similar levels of pyritisation (e.g. Poulton et al., 2015). As such, it is necessary to evaluate additional redox proxies to ensure an accurate interpretation of seawater paleoredox at Macmillan Pass.

Molybdenum Geochemistry

In oxic seawater, molybdenum is present as the conservative molybdate anion (MoO_4^{2-}), which adsorbs onto ferromanganese oxides resulting in a large isotopic fractionation ($\Delta^{98}Mo_{SW-OX} = \delta^{98}Mo_{SW} - \delta^{98}Mo_{OX} \leq 3‰$; Barling et al., 2001; Siebert et al., 2003; Barling and Anbar, 2004; Poulson et al., 2006). In contrast, when sulphide concentrations exceed 11 μM (Erickson and Helz, 2000), the complete transformation of molybdate to reactive thiomolybdate species (substitution of oxygen by sulphur; $MoO_xS_{4-x}^{2-}$) may result in minimal fractionation of $\delta^{98}Mo$ values between sediment and seawater or pore fluid (e.g. Nägler et al., 2005; Neubert et al., 2008). This can also result in high sedimentary Mo enrichments (> 100 ppm) in unrestricted euxinic basins (Scott and Lyons, 2012).

There are currently two studies that provide constraints for the $\delta^{98}Mo$ value of Late Devonian seawater (Gordon et al., 2009; Dahl et al. 2010), albeit from two different periods (Fig. 10). Both studies present data generated from analyses of organic-rich mudstones, where deposition in a euxinic basin is inferred from high levels of pyritisation. The $\delta^{98}Mo$ values reported in either study (~1.5 – 2.0‰) are lower than modern seawater (2.4‰), which provides evidence that the global oceans during the Late Devonian may have been less oxygenated, although it is difficult to accurately constrain the size of the ferruginous vs. euxinic sinks (Gordon et al., 2009; Dahl et al. 2010).

At Macmillan Pass, the narrow distribution of $\delta^{98}Mo$ values (+0.48‰ ± 0.20) is between 0.7‰ and 1.0‰ lower than current constraints for Late Devonian seawater ($\delta^{98}Mo$ = +1.4‰ to +1.6‰; Gordon et al., 2009). Considering the equivocal constraints provided by the Fe based paleoredox proxies, there are three possible explanations for the $\delta^{98}Mo$ values: (1) the Mo has a predominantly hydrothermal rather than authigenic origin; (2) Mo was fractionated from seawater in a non-euxinic setting; (3) deposition occurred in a euxinic setting, with a δ^{98}Mo value of Frasnian seawater that was lower than the constraints for Givetian and Fammenian seawater.

Starting with option (1), the δ^{98}Mo values at Macmillan Pass (Fig. 10) overlap with analyses of modern low-temperature hydrothermal fluids that circulate through sediment covered ridge axis systems (δ^{98}Mo = 0.8‰; McManus et al., 2002). In these modern settings, the Mo is thought to be derived from fluid-rock interaction with basalt (± some diagenetic Mo component; Wheat et al., 2002). The majority of studies on Mo solubility in hydrothermal fluids focus on magmatic hydrothermal systems, where Mo is shown to partition into the vapour phase (Rempel et al., 2009). The hydrothermal systems at Macmillan Pass preserve no evidence of direct magmatic input (Magnall et al., 2016a), and in the hot (> 250°C), reducing ($fO_2 = 10^{-35}$) single phase fluids, Mo^{4+} rather than the more soluble Mo^{6+} will have been stable. The vent fluids are therefore unlikely to have produced a major hydrothermal flux of Mo, which is supported by the negative correlation between Mo and Pb+Zn concentrations in samples from the mineralised vent complex and organic-rich mudstones (Fig. 7). Having established that the Mo in the Macmillan Pass mudstones is predominantly authigenic (rather than hydrothermal), the mechanism of Mo enrichment (option 2) and whether this can provide any information on Late Devonian seawater (option 3) will now be considered.

Organic-rich mudstones commonly preserve a strong relationship between Mo and TOC (Algeo et al. 2007). In modern, strongly restricted, anoxic basins, the efficient transfer of Mo from seawater to sediment results in Mo depletion over time, such that sediments are characterised by low Mo/TOC ratios (e.g. Black Sea; Algeo and Lyons, 2006). Where there is strong co-variation between Mo and TOC, it is also possible to place more quantitative constraints on both the size of the Mo reservoir and also deep-water residence times of Mo within a basin (Algeo et al., 2007). For the Macmillan Pass mudstones, Mo and TOC are only weakly correlated ($r^2 = 0.37$; Fig. 8), with a narrow range in Mo/TOC (3.5 to 8 ppm/wt.%) that overlaps with Black Sea sediments. Similar Mo/TOC values are also preserved in the Richardson Trough samples (Fraser and Hutchison, 2017), although for these samples there is no correlation between Mo and TOC ($r^2 = 0.02$).

The contrasting redox chemistries of Mo and U can lead to the development of characteristic trends that provide information on both the redox and hydrography of depositional environments (Algeo and Tribovillard, 2009). For example, reduction of soluble U^{6+} to insoluble U^{4+} occurs at a similar redox potential to the Fe^{3+}–Fe^{2+} transition, meaning that U enrichment occurs under less reducing conditions than for Mo, which requires sulphidic conditions (Morford et al., 2009). This means that as conditions become more reducing (i.e. suboxic – anoxic – euxinic), there is a progressive enrichment of Mo relative to U in open marine settings (Algeo and Tribovillard, 2009). In contrast, in basins that are both reducing and have longer deep-water renewal times (i.e. basin restriction), water mass chemistry can evolve to lower Mo/U ratios (e.g. Black Sea; Algeo and Tribovillard, 2009). In Figure 11, Mo and U enrichment factors (EFs) have been calculated for samples from Macmillan Pass, and compared to correlative Late Devonian mudstones from the Richardson Trough (Fraser and Hutchison, 2017). The two Selwyn Basin data sets form a linear trend at a Mo/U ratio higher than seawater. This trend is thought to result from the complexation of Mo to Fe and Mn (oxyhydr)oxides (particulate shuttle; Algeo and Tribovillard, 2009), which occurs at the chemocline between oxic and anoxic water masses (Berrang and Grill, 1974; Dellwig et al., 2010). More recently it has been demonstrated that nitrate, not oxygen, can act as the terminal electron acceptor in modern oxygen minimum zones (Scholz et al. 2016); in these settings, Fe^{2+} released from sediment pore fluids is oxidized at the chemocline between weakly sulphidic and nitrogenous conditions in near bottom waters. Importantly, the location of this chemocline exerts a control on the degree of trace element enrichment (Algeo and Tribovillard, 2009). For example, in stratified basins (e.g. the Black Sea) where the chemocline is located high in the water column, particulates undergo reductive dissolution and Mo is released before reaching the sediment (Crusius et al., 1996). In contrast, Mo transfer can be enhanced when there is redox variability on short timescales, particularly when the chemocline is located close to the sediment-water interface (SWI). The suppression of Mo_{EF} values at higher U_{EF} (i.e. a flattening of the Mo-U co-variation), which is a trend typically encountered in strongly restricted basins, is not preserved in the Macmillan Pass samples (Fig. 11). It is worth highlighting that current paleogeographic reconstructions show the Selwyn Basin was no less connected to the global ocean than other Late Devonian basins on the Laurentian margin (Fig. 1). Furthermore, the Mo-U co-variation is similar to trends observed both in moderately restricted basins such as the Cariaco Basin (Venezuela; Algeo and Tribovillard, 2009) and the Baltic Sea (Scholz et al., 2013), as well as upwelling zones in open ocean settings (e.g. Peru; Scholz et al., 2011). This appears to contrast with the low Mo/TOC ratios at Macmillan Pass and Richardson Trough. However, the stronger co-variation between Mo and U demonstrates the predominant mechanism of Mo enrichment occurred via the particulate shuttle, weakening any relationship between Mo and TOC. As such, it may be difficult to make a reliable interpretation of deep-water renewal times when a relationship between Mo and TOC cannot be established.

The particulate shuttle and Mo isotope fractionation

The identification of a particulate shuttle trend provides valuable context for the interpretation of δ^{98}Mo values at Macmillan Pass, which are offset from available constraints for Late Devonian seawater (+1.5 to +2.0‰; Dahl et al., 2010; Gordon et al., 2009). Although Mo isotopes cannot directly help to address the issue of basin restriction, similar isotopic fractionations are preserved in modern anoxic, open-ocean settings (McManus et al., 2002; Poulson et al., 2006; Dickson et al., 2014).

Using the constraints for Late Devonian seawater, the δ^{98}Mo values of the Macmillan Pass mudstones (+0.7 to +1.0‰) correspond with the isotopic fractionation that occurs during Mo adsorption to Fe (oxyhydr)oxides (Goldberg et al., 2009). In samples without major diagenetic pyrite enrichment (Fe/Al < 0.44) there is a positive correlation between Fe/Al and δ^{98}Mo values (Fig. 12a), providing evidence that the redox geochemistry of Fe and Mo may have been linked. A major finding of Goldberg et al. (2009) was that the mineralogy of Fe (oxyhydr)oxides exerts a control on δ^{98}Mo values, as complexation with magnetite, goethite and ferrihydrite produces respective fractionations (Δ^{98}Mo) of 0.83‰ ± 0.60, 1.11‰ ± 0.15 and 1.40‰ ± 0.48. Assuming that δ^{98}Mo values are controlled predominantly by Fe (oxyhydr)oxide mineralogy, the correlation between Fe/Al and δ^{98}Mo values may indicate that a change in mineralogy was accompanied by an increase in delivery of Fe_{HR}.

As sedimentary Mo enrichment appears to be controlled primarily via the particulate shuttle, the correlation between Fe/Al and δ^{98}Mo values could also be explained by a simple closed system Rayleigh fractionation model (Fig. 12b). In terms of the boundary conditions, the model starts with a δ^{98}Mo value of 1.5‰, taken as a lower limit for Late Devonian seawater (Dahl et al., 2010; Gordon et al., 2009). A major assumption of this model is that the δ^{98}Mo value of seawater remained constant throughout the stratigraphic interval, which could represent deposition over more than 7 Myr (Fig. 10). From this starting point (δ^{98}Mo = 1.5‰), a fractionation factor intermediate between ferrihydrite ($\alpha = 0.99989$) and goethite ($\alpha = 0.99986$) is used, which corresponds with the lowermost δ^{98}Mo values at Macmillan Pass (0.33‰). The model then produces the narrow distribution of δ^{98}Mo values without extensive depletion of Mo in the residual fluid (see Fig. 12b). In this case, the residual fluid is unlikely to represent global seawater, the δ^{98}Mo value of which represents isotopic mass balance between all other Mo sinks. Indeed, the good correlation between Fe/Al and δ^{98}Mo is evidence that a single, more localised parameter (i.e. particulate shuttle) is responsible for the isotopic composition of Mo retained in the sediment. Thus, the model demonstrates how the size of the Mo flux associated with the particulate shuttle could produce small corresponding changes in the δ^{98}Mo value of soluble Mo at the chemocline.

Phosphorus cycling and productivity in the Selwyn Basin during the Late Devonian

The anoxic, predominantly non-sulphidic conditions that prevailed at Macmillan Pass during the Late Devonian will have played a key role in the cycling of phosphorus (e.g. März et al., 2008), the availability of which controls primary productivity (Tyrrell, 1999). Unlike Fe, only a minor fraction of the total phosphorus (P_T) in marine sediments is of detrital origin, and a major component of P_T is associated with organic matter and Fe (oxyhydr)oxides (Algeo and Ingall, 2007). Depositional redox conditions, therefore, exert a strong control on the degree to which P is retained within marine sediments, and as conditions become more reducing the regeneration of P from organic matter and Fe (oxyhydr)oxides to seawater is enhanced (Ingall et al., 1993; Ingall and Cappellen, 1990).

The TOC/P ratios of the Macmillan Pass samples are depleted relative to the Redfield ratio (~106:1), which defines the TOC:P ratio of marine phytoplankton (Redfield, 1958). Low TOC/P ratios often develop in sediments deposited under suboxic conditions, when there is limited P regeneration back to the water column (e.g. Peruvian margin; Böning et al., 2004). Moreover, the weak correlation between TOC/P and Mo_{EF} at Macmillan Pass is consistent with the contrasting redox behaviours of P and Mo, with the latter being more sensitive to reduced sulphur availability. Expanding this framework to samples from the Richardson Trough further supports this model; here, high TOC/P values are coupled with more extreme Mo enrichments, indicating extensive P recycling under more reducing (likely sulphidic) conditions.

At Macmillan Pass, the high levels of pyritisation, low TOC/P and intermediate Mo enrichments are similar to those preserved in mudstones deposited in the proto North Atlantic during the Cretaceous under ferruginous conditions (März et al., 2008). Nevertheless, considering the high levels of pyritisation (≥ 0.7) in some Macmillan Pass samples, intermittent periods of euxinia remain a possibility. Notably, continuous high resolution sampling of short stratigraphic intervals has revealed a cyclicity in the development of ferruginous and euxinic conditions during periods of major carbon burial (e.g. März et al., 2008; Poulton et al., 2015). Such redox cyclicity likely has a key role in maintaining a balance between burial and regeneration of P, which ultimately governs P availability, primary productivity and carbon burial over geologic timescales (Van Cappellen and Ingall, 1994). Both at Macmillan Pass and Richardson Trough, the organic rich mudstones are enriched in biogenic silica (>75 wt. %; Magnall et al. 2015, Fraser and Hutchison, 2017), which provides evidence of high productivity during the Late Devonian. The development of anoxic conditions, which were predominantly ferruginous but had potential for intermittent euxinia, would therefore have had an important role in maintaining nutrient availability and productivity on a regional scale.

The role of seawater paleoredox in the formation of SHMS deposits

Some of the early work on seawater paleoredox in the Selwyn Basin emphasised a link between basin restriction, protracted water-column euxinia and sulphide formation (Goodfellow et al., 1993; Turner, 1992). In this euxinic basin model, sulphide formation occurred within the water column following exhalation of hydrothermal fluids above the SWI. However, the Fe speciation and Mo isotope data presented for Macmillan Pass in this study provide no evidence of sustained euxinia. Rather, sulphide was likely restricted to sediment pore fluids with an overlying water column that was predominantly ferruginous.

In ferruginous settings, pyrite formation may be limited by the availability of sulphate rather than organic carbon (Poulton and Canfield, 2011), an observation supported by recent work proposing low concentrations of sulphate in Late Devonian seawater (Sim et al., 2015). Indeed, low seawater sulphate may have been characteristic of much of the Early Paleozoic (Horita et al., 2002). Two factors are important in this context: (1) under reducing conditions, sulphide concentration imposes a limit on the solubility of base metals, and long periods of low seawater sulphate may have facilitated the development of sulphide-poor, Pb-Zn-Fe enriched basinal fluids (Wilkinson, 2014), and; (2) the formation of massive sulphide deposits close to the seafloor in a non-euxinic setting requires the optimisation of other processes that concentrate reduced sulphur, derived from seawater sulphate, into the host rock. Various pathways of sulphur enrichment have been documented in the host rocks to SHMS mineralisation, including diagenetic barite formation (Johnson et al., 2004), diagenetic sulphate reduction (e.g. Fallick et al., 2001; Magnall et al., 2016b), and thermochemical sulphate reduction (Gadd et al., 2016; Magnall et al., 2016a). All pathways are linked by organic carbon, and a common feature of emerging models for SHMS mineralisation is their formation in continental margin environments with high levels of biological productivity (e.g. Magnall et al., 2015; Reynolds et al., 2015; Slack et al., 2016).

Where SHMS deposits form via sub-seafloor replacement, there is clear potential for an overlap between hydrothermal and diagenetic processes. Despite there being no direct modern analogues for SHMS systems, hydrothermal activity in the Guaymas Basin serves as a useful comparison, where rift-related hydrothermal activity is accompanied by the release of methane within recently deposited sediments (Berndt et al., 2016). At Macmillan Pass, SHMS mineralisation occurs where faults provide a flow path for metal-rich hydrothermal fluids (e.g. Magnall et al., 2016a) to reach the shallow sub-surface environment. It is likely, therefore, that the onset and development of hydrothermal activity at Macmillan Pass during the Late Devonian would have resulted in the enhanced circulation of diagenetic fluids in sediments proximal to the hydrothermal system. Clearly, in more dynamic diagenetic environments it is necessary to evaluate multiple proxies when attempting to reconstruct seawater paleoredox. In coupling the Fe and Mo based proxies in samples from a proximal and distal setting (with respect to SHMS mineralisation), we have demonstrated how this approach can be made.

CONCLUSIONS

The co-variation between Mo and U in the combined data-sets from Macmillan Pass and the Richardson Trough provides good evidence that the dominant mechanism of Mo enrichment occurred via a particulate shuttle involving Fe (oxyhydr)oxides. This is further supported by the δ^{98}Mo values preserved in mudstones at Macmillan Pass, which are fractionated from Late Devonian seawater by 0.7 to 1.0 ‰. The incomplete pyritisation of Fe_{HR} ($\leq$ 70%) in samples from DH-76-17 provides evidence that conditions were predominantly ferruginous, with potential for intermittent euxinia. At Macmillan Pass, anoxic, non-sulphidic conditions led to P enrichment and TOC/P ratios below the Redfield ratio (~106:1). This contrasts with the high TOC/P ratios in the Richardson Trough, which are combined with much greater Mo enrichments. Here, regeneration of P within the water column combined with high levels of Mo provides convincing evidence of more persistent water column euxinia. Nevertheless, the dominant mechanism of Mo enrichment was still via the particulate shuttle, and high but uniform Mo/U values provide no evidence of long deep-water renewal times and strong basin restriction. At Macmillan Pass, formation of SHMS deposits in non-euxinic environments therefore requires the optimisation of other factors (e.g. diagenetic sulphate reduction, barite replacement) that contribute to the sulphur budget of the host rock. At a first order, these factors are controlled by high primary productivity and enhanced carbon burial, which therefore represent the most important variables in the development of effective chemical traps for high-grade SHMS deposits.

ACKNOWLEDGEMENTS

The first author would like to thank Romain Guilbaud for his assistance with the Fe speciation experiments. Funding acknowledgement is given to a Helmholtz-Rekrutierungsinitive, and NSERC Discovery Grant to S. Gleeson and the TGI4 initiative (Geological Survey of Canada). Reviews by Thomas Algeo, Nicolas Tribovilliard, Fernando Tornos and in particular the comments of an anonymous reviewer are graciously acknowledged for helping improve the manuscript.

REFERENCES

Abbott, J.G., Turner, R.J., 1991. Character and paleotectonic setting of Devonian stratiform sediment-hosted Zn, Pb, Ba deposits, Macmillan Fold Belt, Yukon, in: Abbott, J.G., Turner, R.J. (Eds.), Geological Survey of Canada Open File 2169. pp. 99–136.

Algeo, T.J., Lyons, T.W., 2006. Mo–total organic carbon covariation in modern anoxic marine environments: Implications for analysis of paleoredox and paleohydrographic conditions. Paleoceanography 21, 1–23.

Algeo, T.J., Ingall, E., 2007. Sedimentary Corg:P ratios, paleocean ventilation, and Phanerozoic atmospheric pO2. Palaeogeog. Palaeoclim. Palaeoeco. 256, 130–155.

Algeo, T.J., Lyons, T.W., Blakey, R.C., Over, J.D., 2007. Hydrographic conditions of the Devono–Carboniferous North American Seaway inferred from sedimentary Mo–TOC relationships. Palaeogeog. Palaeoclim. Palaeoeco. 256, 204–230.

Algeo, T.J., Tribovillard, N., 2009. Environmental analysis of paleoceanographic systems based on molybdenum–uranium covariation. Chem. Geol. 268, 211–225.

Arnold, G.L., Anbar, A.D., Barling, J., Lyons, T.W., 2004. Molybdenum Isotope Evidence for Widespread Anoxia in Mid-Proterozoic Oceans. Science 304, 87–90.

Barling, J., Anbar, A.D., 2004. Molybdenum isotope fractionation during adsorption by manganese oxides. Earth Planet. Sci. Lett. 217, 315–329.

Barling, J., Arnold, G.L, Anbar, A.D, 2001. Natural mass-dependent variations in the isotopic composition of molybdenum. Earth Planet. Sci. Lett. 193, 447–457.

Berndt, C., Hensen, C., Mortera-Gutierrez, C., Sarkar, S., Geilert, S., Schmidt, M., Liebetrau, V., Kipfer, R., Scholz, F., Doll, M., Muff, S., Karstens, J., Planke, S., Petersen, S., Böttner, C., Chi, W.C., Moser, M., Behrendt, R., Fiskal, A., Lever, M.A., Su, C.C., Deng, L., Brennwald, M.S., Lizarralde, D., 2016. Rifting under steam - how rift magmatism triggers methane venting from sedimentary basins. Geology 44, 767–770.

Berrang, P.G., Grill, E. V., 1974. The effect of manganese oxide scavenging on molybdenum in saanich inlet, British Columbia. Mar. Chem. 2, 125–148.

Blakey, R., 2013. Late Devonian from Map Series. North American Key Time Slices © 2013 Colorado Plateau Geosystems Inc.

Böning, P., Brumsack, H.-J., Böttcher, M.E., Schnetger, B., Kriete, C., Kallmeyer, J., Borchers, S.L., 2004. Geochemistry of Peruvian near-surface sediments. Geochim. Cosmochim. Acta 68, 4429–4451.

Borowski, W.S., Rodriguez, N.M., Paull, C.K., Ussler, W., 2013. Are 34S-enriched authigenic sulfide minerals a proxy for elevated methane flux and gas hydrates in the geologic record? Mar. Pet. Geol. 43, 381–395.

Canfield, D.E., Raiswell, R.R., Westrich, J.T., Reaves, C.M., Berner, R.A., 1986. The use of chromium reduction in the analysis of reduced inorganic sulfur in sediments and shales. Chem. Geol. 54, 149–155.

Carne, R.C., Cathro, R.J., 1982. Sedimentary exhalative (sedex) zinc-lead-silver deposits, northern Canadian Cordillera. Can. Min. Metall. Bull. 75, 66–78.

Clarkson, M.O., Poulton, S.W., Guilbaud, R., Wood, R.A., 2014. Assessing the utility of Fe/Al and Fe-speciation to record water column redox conditions in carbonate-rich sediments. Chem. Geol. 382, 111–122.

Crusius, J., Calvert, S., Pedersen, T., Sage, D., 1996. Rhenium and molybdenum enrichments in sediments as indicators of oxic, suboxic and sulfidic conditions of deposition. Earth Planet. Sci. Lett. 145, 65–78.

Dahl, T.W., Hammarlund, E.U., Anbar, A.D., Bond, D.P.G., Gill, B.C., Gordon, G.W., Knoll, A.H., Nielsen, A.T., Schovsbo, N.H., Canfield, D.E., 2010. Devonian rise in atmospheric oxygen correlated to the radiations of terrestrial plants and large predatory fish. Proc. Natl. Acad. Sci. U.S.A. 107, 17911–17915.

Dellwig, O., Leipe, T., März, C., Glockzin, M., Pollehne, F., Schnetger, B., Yakushev, E. V., Böttcher, M.E., Brumsack, H.-J., 2010. A new particulate Mn–Fe–P-shuttle at the redoxcline of anoxic basins. Geochim. Cosmochim. Acta 74, 7100–7115.

Dickson, A.J., Cohen, A.S., Coe, A.L., 2014. Continental margin molybdenum isotope signatures from the early Eocene. Earth and Planetary Science Letters. 404, 389–395.

Duan, Y., Anbar, A.D., Arnold, G.L., Lyons, T.W., Gordon, G.W., Kendall, B., 2010. Molybdenum isotope evidence for mild environmental oxygenation before the Great Oxidation Event. Geochim. Cosmochim. Acta 74, 6655–6668.

Emerson, S.R., Huested, S.S., 1991. Ocean anoxia and the concentrations of molybdenum and vanadium in seawater. Mar. Chem. 34, 177–196.

Erickson, B.E., Helz, G.R., 2000. Molybdenum(VI) speciation in sulfidic waters: Stability and lability of thiomolybdates. Geochim. Cosmochim. Acta 64, 1149–1158.

Fallick, A.E., Ashton, J.H., Boyce, A.J., Ellam, R.M., Russell, M.J., 2001. Bacteria were responsible for the magnitude of the world-class hydrothermal base metal sulfide orebody at Navan, Ireland. Econ. Geol. 96, 885–890.

Fraser, T.A., Hutchison, M.P., 2017. Lithogeochemical characterization of the Middle – Upper Devonian Road River Group and Canol and Imperial formations on Trail River, east Richardson Mountains, Yukon: age constraints and a depositional model for fine-grained strata in the Lower Paleozoic Richardson Trough. Can. Journ. Earth Sci. 54, 731–765.

Gadd, M.G., Layton-Matthews, D., Peter, J.M., Paradis, S., Jonasson, I.R., 2016. The world-class Howard’s Pass SEDEX Zn-Pb district, Selwyn Basin, Yukon. Part II: the roles of thermochemical and bacterial sulfate reduction in metal fixation. Miner. Depos. 1–15.

Goldberg, T., Archer, C., Vance, D., Poulton, S.W., 2009. Mo isotope fractionation during adsorption to Fe (oxyhydr)oxides. Geochim. Cosmochim. Acta 73, 6502–6516.

Goldberg, T., Gordon, G., Izon, G., Archer, C., Pearce, C.R., McManus, J., Anbar, A.D., Rehkämper, M., 2013. Resolution of inter-laboratory discrepancies in Mo isotope data: an intercalibration. Journ. Anal. At. Spect. 28, 724–735.

Gomes, M.L., Hurtgen, M.T., 2015. Sulfur isotope fractionation in modern euxinic systems:

Implications for paleoenvironmental reconstructions of paired sulfate–sulfide isotope records. Geochim. Cosmochim. Acta 157, 39–55.

Goodfellow, W.D., 1987. Anoxic Stratified Oceans as a Source of Sulphur in Sediment-Hosted Stratiform Zn-Pb Deposits (Selwyn Basin, Yukon, Canada). Chem. Geol. (Isotope Geosci. Sect. 65, 359–382.

Goodfellow, W.D., Lydon, J.W., Turner, R.J., 1993. Geology and genesis of stratiform sediment-hosted (SEDEX) zinc-lead-silver sulphide deposits, in: Kirkham, R.W., Sinclair, R., Thorpe, R.I., Duke, J.M. (Eds.), Mineral Deposit Modeling. Geological Association of Canada, pp. 201–252.

Gordey, S.P., Anderson, R.G., 1993. Evolution of the northern cordilleran miogeocline, Nahanni map area (105I), Yukon and Northwest Territories, Memoir 428. ed. Geological Survey of Canada.

Gordon, G.W., Lyons, T.W., Arnold, G.L., Roe, J., Sageman, B.B., Anbar, A.D., 2009. When do black shales tell molybdenum isotope tales? Geology 37, 535–538.

Gromet, L.P., Haskin, L. a., Korotev, R.L., Dymek, R.F., 1984. The “North American shale composite”: Its compilation, major and trace element characteristics. Geochim. Cosmochim. Acta 48, 2469–2482.

Harris, N.B., Mnich, C. a., Selby, D., Korn, D., 2013. Minor and Trace Element and Re-Os Chemistry of the Upper Devonian Woodford Shale, Permian Basin, West Texas: Insights into Metal Abundance and Basin Processes. Chem. Geol. 356, 76–93.

Horita, J., Zimmerman, H., Holland, H.D., 2002. Chemical evolution of seawater during the Phanerozoic: Implications from the record of marine evaporites. Geochim. Cosmochim. Acta 66, 3733–3756.

House, M.R., 2002. Strength, timing, setting and cause of mid-Palaeozoic extinctions. Palaeogeog. Palaeoclim. Palaeoeco. 181, 5–25.

Ingall, E.D., Bustin, R.M., Van Cappellen, P., 1993. Influence of water column anoxia on the burial and preservation of carbon and phosphorus in marine shales. Geochim. Cosmochim. Acta 57, 303–316.

Ingall, E.D., Cappellen, P. Van, 1990. Relation between sedimentation rate and burial of organic phosphorus and organic carbon in marine sediments. Geochim. Cosmochim. Acta 54, 373–386.

Johnson, C.A., Kelley, K.D., Leach, D.L., 2004. Sulfur and Oxygen Isotopes in Barite Deposits of the Western Brooks Range, Alaska, and Implications for the Origin of the Red Dog Massive Sulfide Deposits. Econ. Geol. 99, 1435–1448.

Kaufmann, B., 2006. Calibrating the Devonian Time Scale: A synthesis of U-Pb ID-TIMS ages and conodont stratigraphy. Earth-Science Rev. 76, 175–190.

Lin, Z., Sun, X., Lu, Y., Strauss, H., Xu, L., Gong, J., Teichert, B.M.A., Lu, R., Lu, H., Sun, W., Peckmann, J., 2016. The enrichment of heavy iron isotopes in authigenic pyrite as a possible indicator of sulfate-driven anaerobic oxidation of methane: Insights from the South China Sea. Chem. Geol. 449, 15–29.

Lyons, T.W., Gellatly, A.M., Mcgoldrick, P.J., Kah, L.C., 2006. Proterozoic sedimentary exhalative (SEDEX) deposits and links to evolving ocean chemistry. Geol. Soc. Am. Mem. 198, 169–184.

Lyons, T.W., Severmann, S., 2006. A critical look at iron paleoredox proxies: New insights from modern euxinic marine basins. Geochim. Cosmochim. Acta 70, 5698–5722.

Magnall, J.M., Gleeson, S.A., Paradis, S., 2015. The importance of siliceous radiolarian-bearing mudstones in the formation of sediment-hosted Zn-Pb ± Ba mineralization in the Selwyn Basin, Yukon, Canada. Econ. Geol. 110, 2139–2146.

Magnall, J.M., Gleeson, S.A., Blamey, N.J.F., Paradis, S., Luo, Y., 2016a. The thermal and chemical evolution of hydrothermal vent fluids in shale hosted massive sulphide (SHMS) systems from the MacMillan Pass district (Yukon, Canada). Geochim. Cosmochim. Acta 193, 251–273.

Magnall, J.M., Gleeson, S.A., Stern, R.A., Newton, R.J., Poulton, S.W., Paradis, S., 2016b. Open system sulphate reduction in a diagenetic environment – isotopic analysis of barite (δ 34S and δ 18O) and pyrite (δ 34S) from the Tom and Jason Late Devonian Zn-Pb-Ba deposits, Selwyn Basin, Canada. Geochim. Cosmochim. Acta 180, 146–163.

März, C., Poulton, S.W., Beckmann, B., Küster, K., Wagner, T., Kasten, S., 2008. Redox sensitivity of P cycling during marine black shale formation: Dynamics of sulfidic and anoxic, non-sulfidic bottom waters. Geochim. Cosmochim. Acta 72, 3703–3717.

McLennan, S., 2001. Relationships between the trace element composition of sedimentary rocks and upper continental crust. Geochem. Geophy. Geosys. 2. 2000GC000109.

McManus, J., Nägler, T.F., Siebert, C., Wheat, C.G., Hammond, D.E., 2002. Oceanic molybdenum isotope fractionation: Diagenesis and hydrothermal ridge-flank alteration. Geochemistry, Geophys. Geosystems 3, 1–9.

Morford, J.L., Martin, W.R., Carney, C.M., 2009. Uranium diagenesis in sediments underlying bottom waters with high oxygen content. Geochim. Cosmochim. Acta 73, 2920–2937.

Nägler, T.F., Siebert, C., Lüschen, H., Böttcher, M.E., 2005. Sedimentary Mo isotope record across the Holocene fresh-brackish water transition of the Black Sea. Chem. Geol. 219, 283–295.

Nägler, T.F., Anbar, A.D., Archer, C., Goldberg, T., Gordon, G.W., Greber, N.D., Siebert, C., Sohrin, Y., Vance, D., 2014. Proposal for an international molybdenum isotope measurement standard and data representation. Geostand. and Geoanalyt. Res. 38, 149–151.

Nelson, J., Colpron, M., 2007. Tectonics and metallogeny of the British Columbia, Yukon and Alaskan Cordillera, 1.8 Ga to the present. Miner. Depos. Canada A Synth. Major Depos. Dist. Metallog. Evol. Geol. Prov. Explor. Methods 2703, 755–791.

Neubert, N., Nägler, T.F., Böttcher, M.E., 2008. Sulfidity controls molybdenum isotope fractionation into euxinic sediments: Evidence from the modern Black Sea. Geology 36, 775–778.

Newton, R.J., Reeves, E.P., Kafousia, N., Wignall, P.B., Bottrell, S.H., Sha, J.-G., 2011. Low marine sulfate concentrations and the isolation of the European epicontinental sea during the Early Jurassic. Geology 39, 7–10.

Ohmoto, H., Goldhaber, M.B., 1997. Sulfur and Carbon Isotopes, in: Barnes, H.L. (Ed.), Geochemistry of Hydrothermal Ore Deposits. John Wiley & Sons, pp. 517–612.

Poulson, R.L., Siebert, C., McManus, J., Berelson, W.M., 2006. Authigenic molybdenum isotope signatures in marine sediments. Geology 34, 617–620.

Poulson Brucker, R.L., McManus, J., Severmann, S., Berelson, W.M., 2009. Molybdenum behavior during early diagenesis: Insights from Mo isotopes. Geochemistry, Geophys. Geosystems 10, 1–25.

Poulton, S., Canfield, D., 2005. Development of a sequential extraction procedure for iron: implications for iron partitioning in continentally derived particulates. Chem. Geol. 214, 209–221.

Poulton, S.W., Canfield, D.E., 2011. Ferruginous Conditions: A Dominant Feature of the Ocean through Earth’s History. Elements 7, 107–112.

Poulton, S.W., Henkel, S., März, C., Urquhart, H., Flögel, S., Kasten, S., Sinninghe Damsté, J.S., Wagner, T., 2015. A continental-weathering control on orbitally driven redox-nutrient cycling during Cretaceous Oceanic Anoxic Event 2. Geology 43, 963–966.

Poulton, S.W., Raiswell, R., 2002. The low-temperature geochemical cycle of iron: from continental fluxes to marine sediment deposition. Am. J. Sci. 302, 774–805.

Raiswell, R., Canfield, D.E., 1998. Sources of iron for pyrite formation in marine sediments. Am. J. Sci. 298, 219–245.

Redfield, A.C., 1958. The biological control of chemical factors in the environment. Am. Sci. 46, 205–222.

Rempel, K.U., Williams-Jones, A.E., Migdisov, A.A., 2009. The partitioning of molybdenum(VI) between aqueous liquid and vapour at temperatures up to 370C. Geochim. Cosmochim. Acta 73, 3381–3392.

Reynolds, M.A., Gingras, M.K., Gleeson, S.A., Stemler, J.U., 2015. More than a trace of oxygen: Ichnological constraints on the formation of the giant Zn-Pb-Ag ± Ba deposits, Red Dog district, Alaska. Geology 43, 867–870.

Scholz, F., Hensen, C., Noffke, A., Rohde, A., Liebetrau, V., Wallmann, K., 2011. Early diagenesis of redox-sensitive trace metals in the Peru upwelling area – response to ENSO-related oxygen fluctuations in the water column. Geochim. Cosmochim. Acta 75, 7257–7276.

Scholz, F., Löscher, C.R., Fiskal, A., Sommer, S., Hensen, C., Lomnitz, U., Wuttig, K., Göttlicher, J., Kossel, E., Steininger, R., Canfield, D.E., 2016. Nitrate-dependent iron oxidation limits iron transport in anoxic ocean regions. Earth Planet. Sci. Lett. 454, 272–281.

Scholz, F., McManus, J., Sommer, S., 2013. The manganese and iron shuttle in a modern euxinic basin and implications for molybdenum cycling at euxinic ocean margins. Chem. Geol. 355, 56–68.

Scholz, F., Severmann, S., McManus, J., Hensen, C., 2014. Beyond the Black Sea paradigm: The sedimentary fingerprint of an open-marine iron shuttle. Geochim. Cosmochim. Acta 127, 368–380.

Scott, C., Lyons, T.W., 2012. Contrasting molybdenum cycling and isotopic properties in euxinic versus non-euxinic sediments and sedimentary rocks: Refining the paleoproxies. Chem. Geol. 324–325, 19–27.

Siebert, C., McManus, J., Bice, A., Poulson, R., Berelson, W.M., 2006. Molybdenum isotope signatures in continental margin marine sediments. Earth Planet. Sci. Lett. 241, 723–733.

Siebert, C., Nägler, T.F., von Blanckenburg, F., Kramers, J.D., 2003. Molybdenum isotope records as a potential new proxy for paleoceanography. Earth Planet. Sci. Lett. 211, 159–

171.

Sim, M.S., Ono, S., Hurtgen, M.T., 2015. Sulfur isotope evidence for low and fluctuating sulfate levels in the Late Devonian ocean and the potential link with the mass extinction event. Earth Planet. Sci. Lett. 419, 52–62.

Slack, J.F.., Falck, H., Kelley, K.D., Xue, G.G., 2016. Geochemistry of host rocks in the Howards Pass district, Yukon-Northwest Territories, Canada: implications for sedimentary environments of Zn-Pb and phosphate mineralization. Miner. Depos. 52, 565–593.

Turner, E.C., Roots, C.F., MacNaughton, R.B., Long, D.G.F., Fischer, B.J., Gordey, S.P., Martel, E., Pope, M.C., 2011. Chapter 3. Stratigraphy, in: Martel, E., Turner, E.C., Fischer, B.. (Eds.), Geology of the Central Mackenzie Mountains of the North Canadian Cordillera, Sekwi Mountain (105P), Mount Eduni (106A), and Northwestern Wrigley Lake (95M) Map-Areas, Northwest Territories. NWT Geoscience Office, pp. 31–192.

Turner, R.J.W., 1992. Formation of Phanerozoic stratiform sediment , hosted zinc- lead deposits : Evidence for the critical role of ocean anoxia. Chem. Geol. 99, 165–188.

Tyrrell, T., 1999. The relative in inluences of nitrogen and phosphorus on oceanic primary production. Nature 400, 525–530.

Van Cappellen, P., Ingall, E.D., 1994. Benthic phosphorus regeneation, net primary production,and ocean anoxia: A model of the coupled marine biogeochemical cycles of carbon and phosphorus. Paleoceanography 9, 677–692.

Wheat, C.G., Mottl, M.J., Rudnicki, M., 2002. Trace element and REE composition of a low-temperature ridge-flank hydrothermal spring. Geochim. Cosmochim. Acta 66, 3693–3705.

Wilkinson, J.J., 2014. Sediment-Hosted Zinc–Lead Mineralization: Processes and Perspectives, in: Treatise on Geochemistry: Second Edition. Elsevier Ltd., pp. 219–249.

Figure 1. The paleogeography of North America (Laurentia) during the Late Devonian (380 – 370 Ma). Cross section A – B taken from Nelson and Colpron (2007) and paleogeography reconstruction annotated from Blakey (2016). The black stars correspond with lithogeochemical studies conducted on organic-rich mudstones from broadly time equivalent Late Devonian basins: (1) Selwyn Basin (this study), (2) Western Canadian Sedimentary Basin (Algeo et al., 2007), (3) Illinois Basin (Dahl et al. 2010), (4) Appalachian Basin (Gordon et al. 2009), (5) Permian Basin (Harris et al., 2013).

Figure 2. A – The regional extent of the Selwyn Basin in the Canadian Cordillera with the locations of major sediment hosted massive sulphide deposits (modified from Nelson and Colpron, 2007). Allochthonous terranes accreted during Mesozoic deformation occur west of the Tintina Fault; east of this regional structure is the Selwyn Basin and adjoining carbonate platform that formed a passive margin along the western margin of ancestral North America (Laurentia). B – A stratigraphic column for the Selwyn Basin, compiled from work mostly conducted at Macmillan Pass (Abbott and Turner, 1991; Carne and Cathro, 1982; Gordey and Anderson, 1993; Turner et al., 2011). C – The local geology at Macmillan Pass, along with the location of the drill-holes from which samples were obtained in this study (modified from Abbott and Turner, 1991).

Figure 3. Lithological sedimentary logs for drill holes TYK-1, 76-17 and TYK-5 with sample locations annotated by grey arrows. The un-mineralised drill-hole (76-17) has been correlated with two drill-holes intersecting sulphide mineralisation at the Tom deposit, and is described in further detail in Magnall et al. (2015). In TYK-1, the vent complex occurs beneath the bedded mineralisation.

Figure 4. Photographs of un-mineralised mudstone samples from 76-17 and TYK-5, and a sample of the hydrothermal vent from TYK-1. The areas from which lithogeochemical analyses were produced are highlighted by the white boxes and those for thin sections by the red boxes.

Figure 5. Lithological logs, Fe speciation (Fe_{PY}/Fe_{HR} and Fe_{HR}/Fe_{T}) and Mo geochemical data (abundance and $\delta^{98}Mo$ values) for DH-7617 (A) and DH-TYK5 (B). All samples plot within the anoxic field ($Fe_{HR}/Fe_{T} > 0.38$), and samples from TYK-5 contain a higher proportion of pyritised reactive Fe ($Fe_{PY}/Fe_{HR} > 0.8$). A thick black line represents Late Devonian seawater ($\delta^{98}Mo = 1.5 \pm 0.1$ ‰) and the grey dashed line represents Mo enrichment in euxinic settings (Scott and Lyons, 2012).

Figure 6. A – histogram of Fe/Al for mudstones from DH-76-17 and DH-TYK-5, compared with mudstones from the Richardson Trough (Fraser and Hutchison, 2017). B – Fe_{PY}/Fe_{HR} vs. $\delta^{34}S$ values (Magnall et al. 2016b) in samples from 76-17 (hollow) and TYK-5 (solid).

Figure 7. Box and whisker plots for Pb, Zn and Mo in mudstone samples from 76-17 (grey), TYK-5 (black) and the mineralised vent (orange). Circles and lines denote the median and average, respectively, and whiskers extend to outliers beyond the 1st and 3rd quartiles.

Figure 8. TOC vs. Mo (ppm) for samples from Macmillan Pass (this study) and the Richardson Trough (Fraser and Hutchison, 2017).

Figure 9. A – Log TOC/P (molar ratio) vs. Log Mo_{EF} for Macmillan Pass mudstones and Richardson Trough samples. Box and whisker plots for the sample sub-groups are included at the

top of the figure (note the different axis), with boxes representing the interquartile range, white circles the average and outliers (1.5 * Q3 – Q1) data that plots beyond the whiskers. B – Log TOC/P (molar ratio) vs. Log P/Al (wt. %) for Macmillan Pass mudstones and Richardson Trough samples. Separate regression lines (dotted) are plotted for Macmillan Pass and Richardson Trough samples, and also for the combined data set (solid).

Figure 10. Chronostratigraphy of the Late Devonian with annotated conodant biostratigraphy (Kaufmann, 2006), mass extinction events (House, 2002) and published δ^{98}Mo values (this study; Gordon et al., 2009; Dahl et al. 2010). The isotopic fractionation of Mo between Late Devonian seawater (δ^{98}Mo = 1.5 ± 0.1 ‰) and sediment deposited in contrasting redox environments ($\Delta^{98}\mathrm{Mo}_{\mathrm{SW\text{-}SED}}$): euxinic (Neubert et al., 2008), anoxic (Poulson et al., 2006; Poulson Brucker et al., 2009), suboxic and oxic (Siebert et al., 2006), and the suggested δ^{98}Mo value for low-temperature hydrothermal fluids (McManus et al., 2002).

Figure 11. The abundance of Mo and U for Macmillan Pass and Richardson Trough mudstones calculated as enrichment factors ($X_{EF} = (X/Al)_{sample} / (X/Al)_{NASC}$), where NASC = North American Shale Composite (Gromet et al., 1984). The annotated redox states (suboxic, anoxic and euxinic) correspond with the observation that relative to seawater (sw), Mo enrichment exceeds U enrichment in progressively reducing conditions; however, more extreme enrichment of Mo over U also occurs during particulate shuttling of Fe-Mn oxyhydr(oxides), when these complexes are deposited and subsequently dissolved during early diagenesis (Algeo and Tribovillard, 2009).

Figure 12. A – δ^{98}Mo vs. Fe/Al for Macmillan Pass mudstones. Samples with low Fe/Al (< 0.44) preserve a good correlation ($r^2 = 0.82$) between δ^{98}Mo and Fe/Al. Samples located within 15 meters of the mineralised interval in DH-TYK-5 form another sub-group, as they preserve

evidence of post depositional pyrite enrichment and phyllosilicate alteration associated with the hydrothermal system (described in Magnall et al. 2015). B – closed system Rayleigh fractionation model describing the evolution of $\delta^{98}Mo_{fluid}$ values that occurs with progressive complexation of Mo to Fe (oxyhydr)oxides. The upper and lower dotted lines represent goethite and ferrihydrite respectively; the solid line represents a fractionation factor intermediate between the two.

Figure1

Click here to download high resolution image

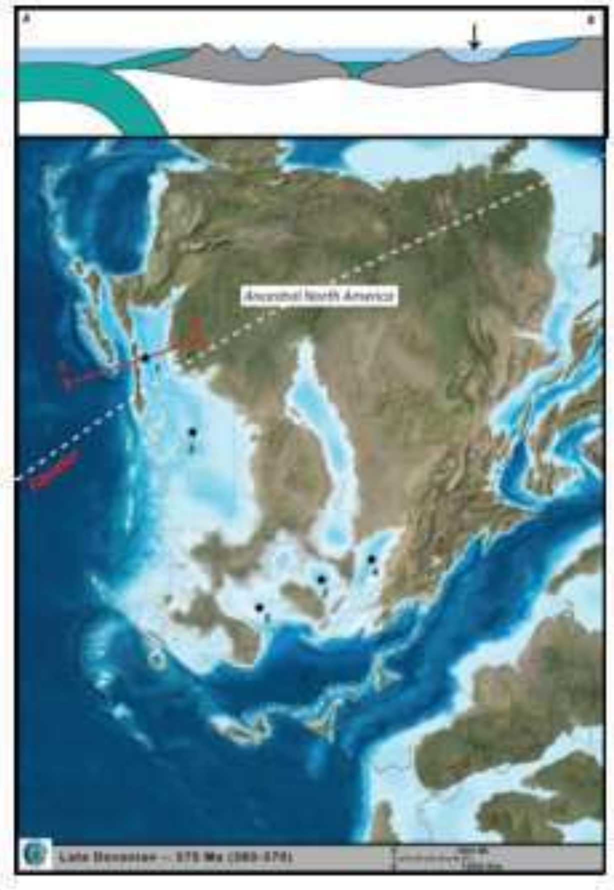

Figure2

Click here to download high resolution image

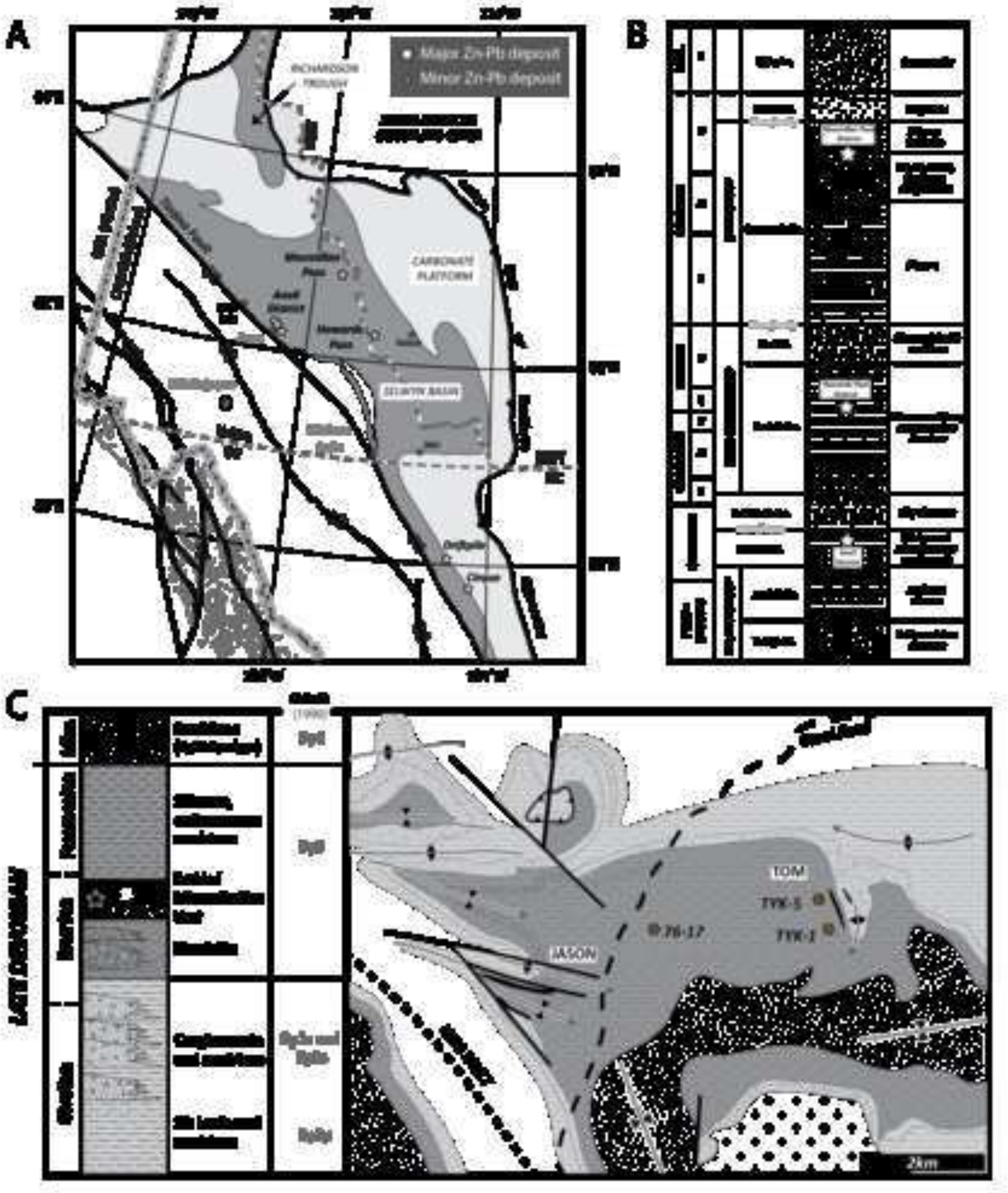

Figure3

Click here to download high resolution image

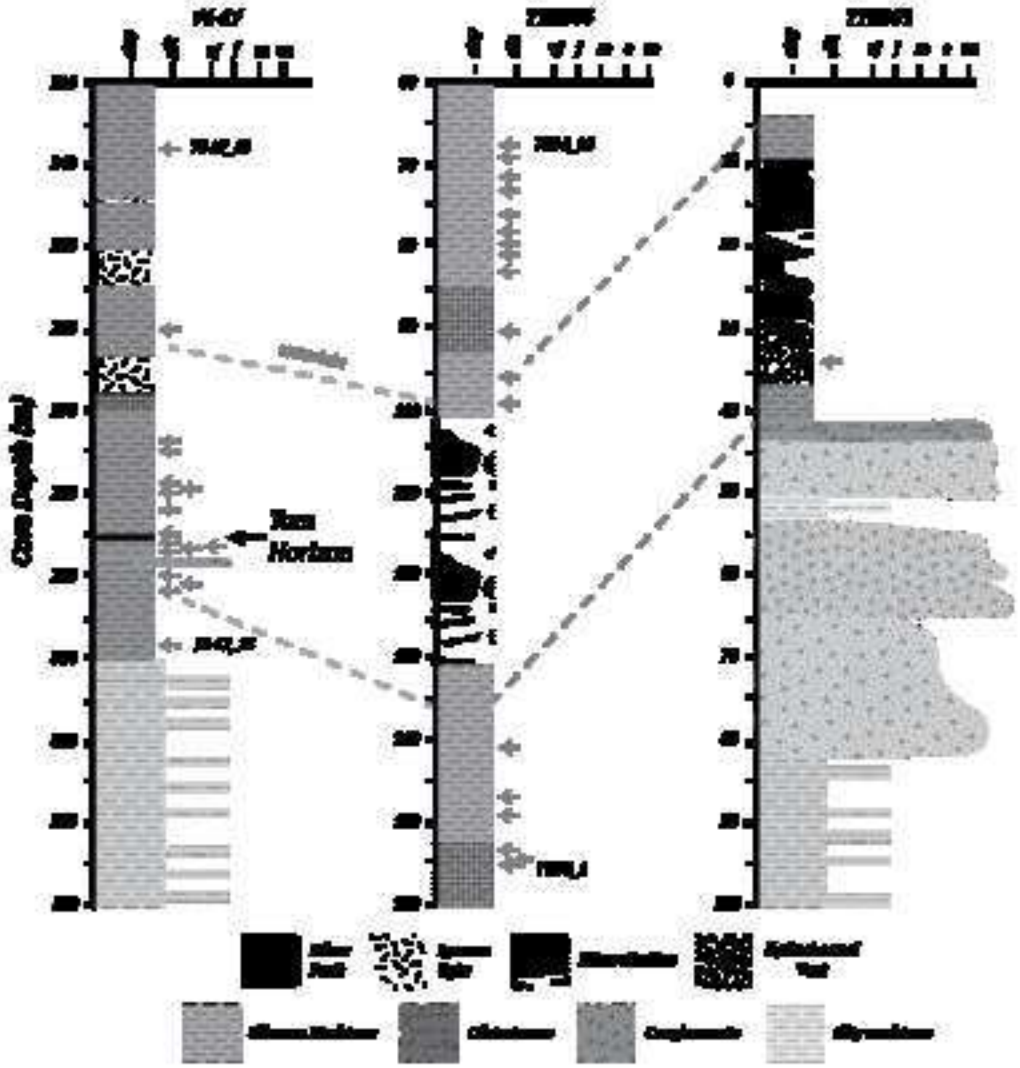

Figure5

Click here to download high resolution image

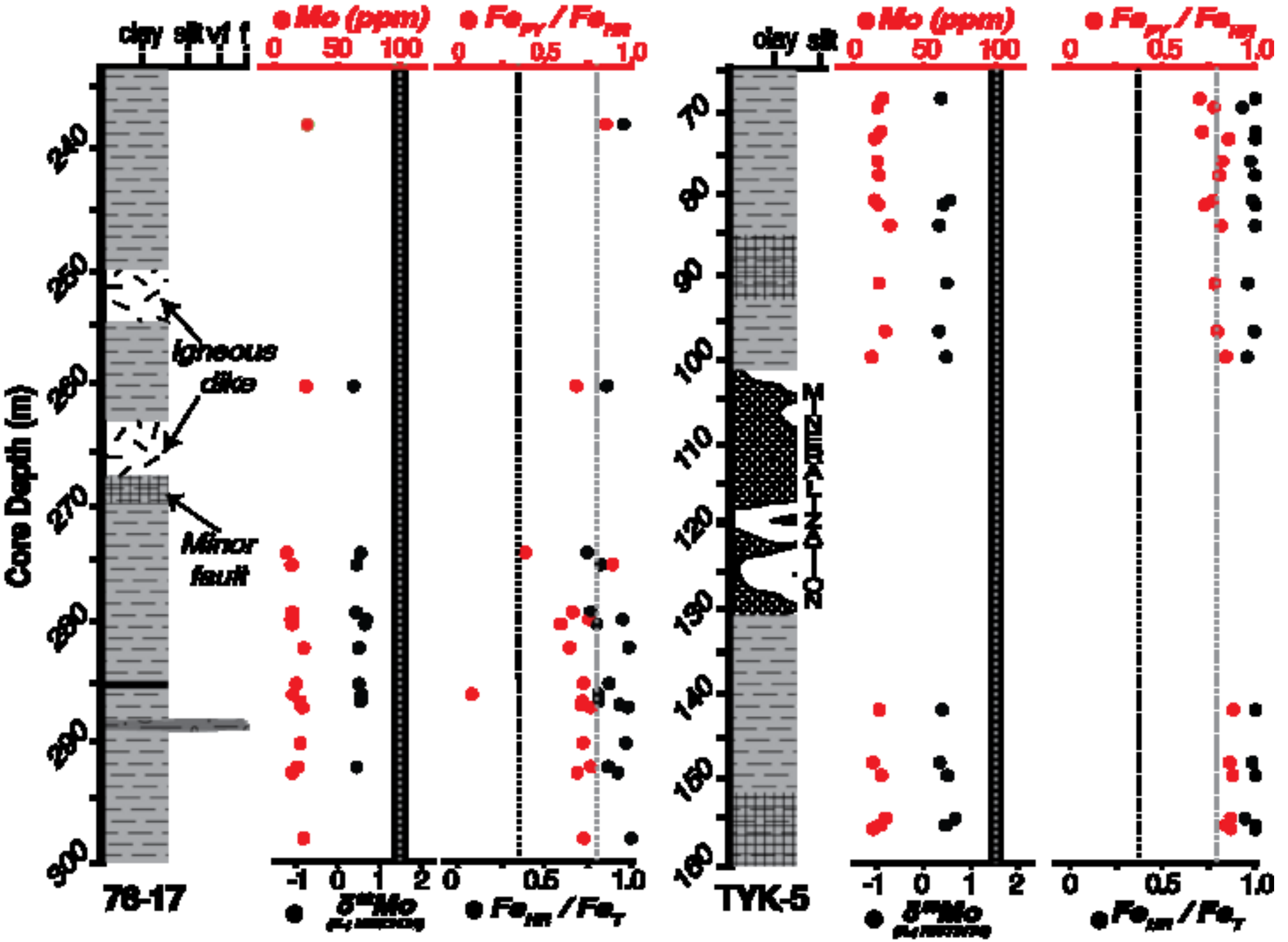

Figure 6

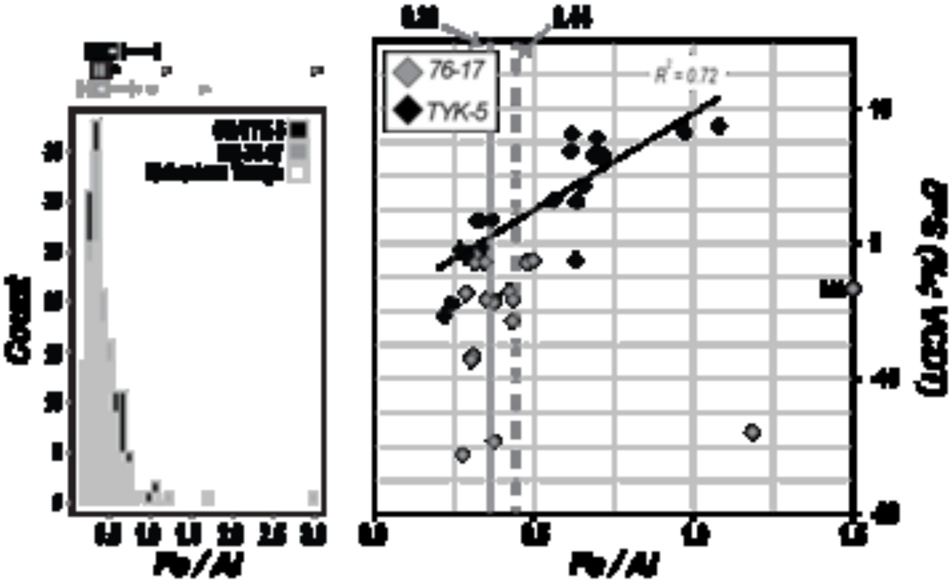

Figure7

Figure 6

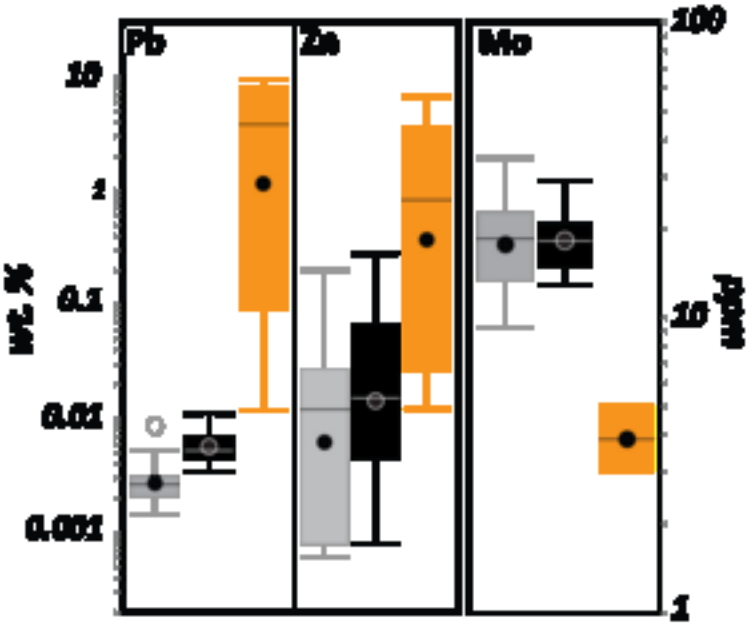

Figure8

Figure 8

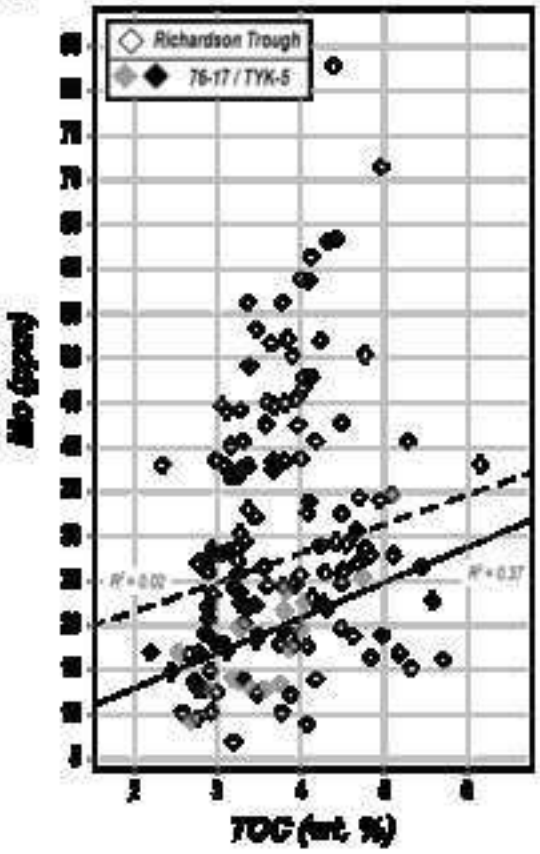

Figure9

Figure 9

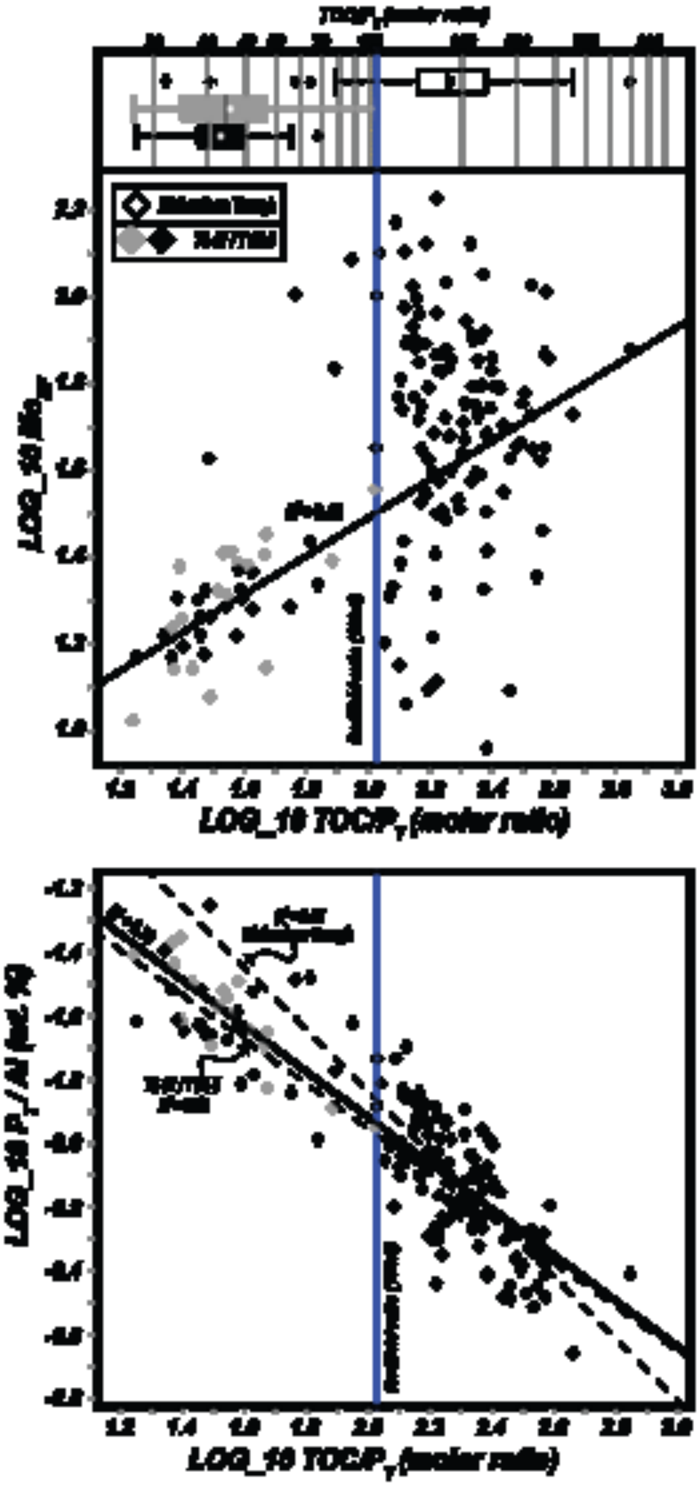

Figure10

Figure 10

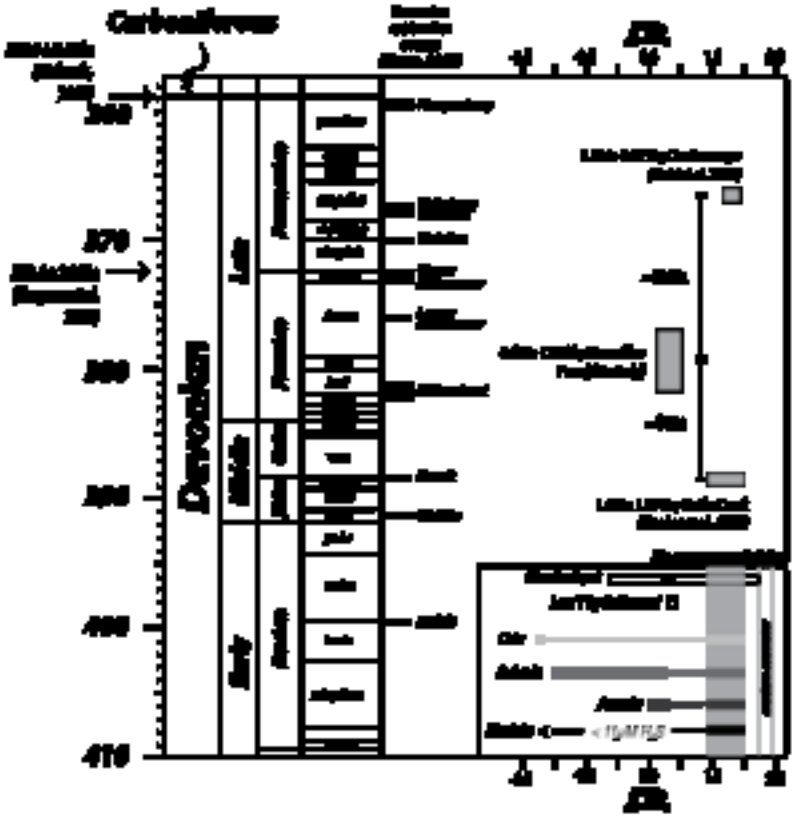

Figure11

Figure 11

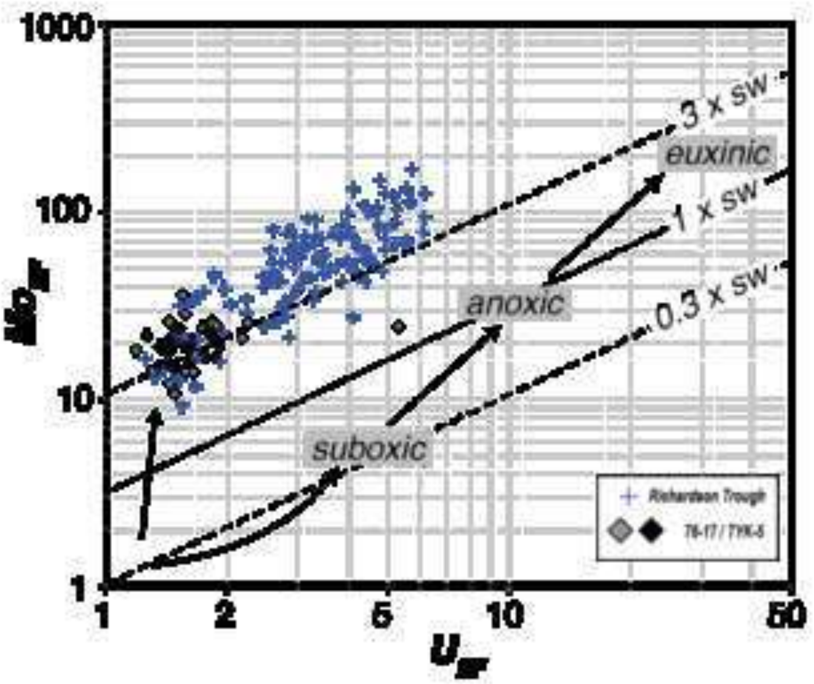

Figure 12

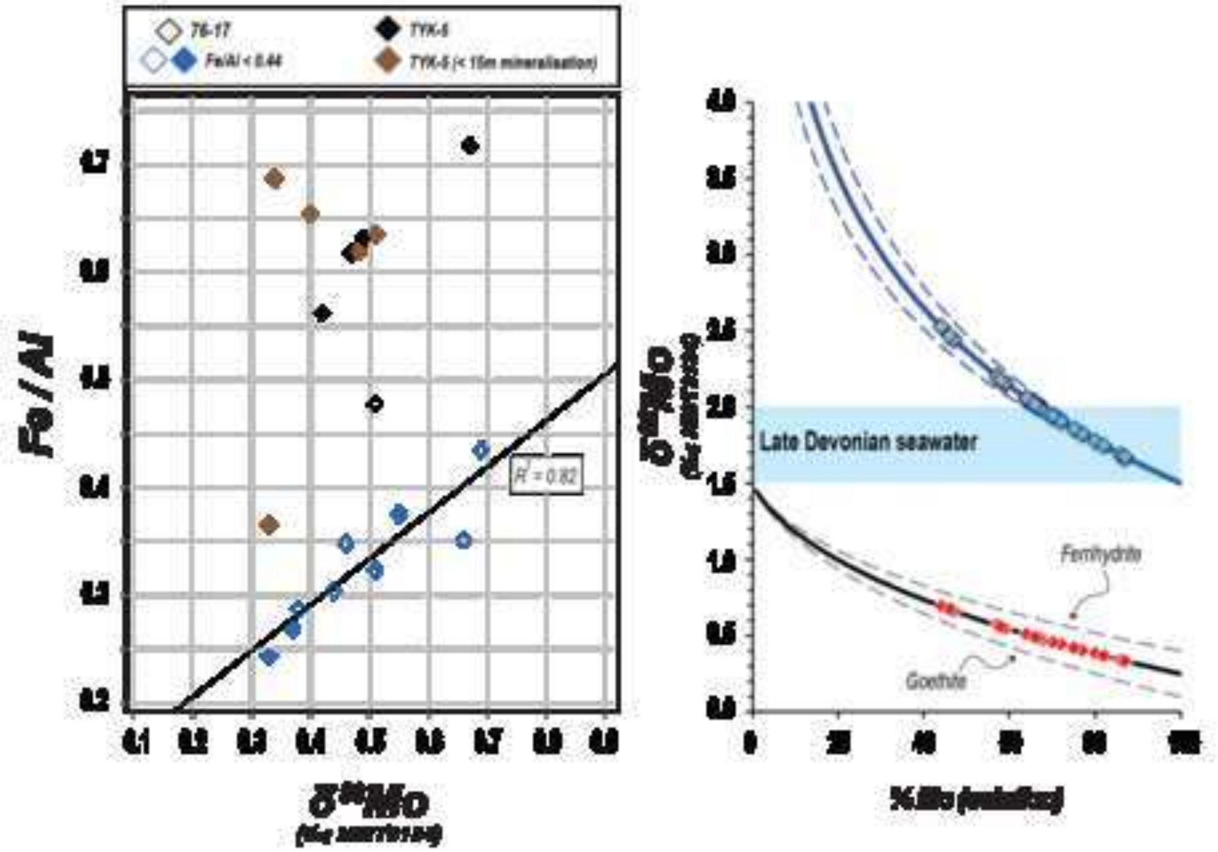
76-17
TYK-5
Fe/Al < 0.44
TYK-5 (< 15m mineralisation)
Fe / Al
0.2
0.3
0.4
0.5
0.6
0.7
0.1
0.2
0.3
0.4
0.5
0.6
0.7
0.8
0.9
R^2 = 0.82
δ^{98}Mo
δ^{98}Mo
4.0
3.5
3.0
2.5
2.0
1.5
1.0
0.5
0.0
Late Devonian seawater
Ferrihydrite
Goethite
0
20
40
60
80
100

Table1

Sample #	Metres	C_{org}	P	S_T	Al_T	Fe_T	Pb	Zn	Mo	U	Mo_{EF}	U_{EF}
				wt. %				*ppm*				
76-17_15	*298*	4.0	0.1	1.1	3.9	1.7	43.0	227.0	22.5	6.1	25.6	2.2
76-17_17	*292.5*	3.4	0.1	0.8	3.4	1.1	26.5	587.0	13.1	3.9	17.2	1.7
76-17_18	*292*	3.9	0.1	1.1	3.8	1.3	29.7	276.0	17.5	4.9	20.5	1.8
76-17_20	*290*	3.3	0.1	1.2	3.5	1.5	30.9	226.0	19.9	4.4	25.6	1.8
76-17_22	*287*	3.8	0.1	1.3	4.0	1.5	29.8	521.0	21.7	5.3	23.9	1.9
76-17_23	*286.8*	4.0	0.2	0.9	3.6	1.1	20.4	173.0	19.6	4.4	23.9	1.7
76-17_24	*286.5*	3.3	0.1	0.9	3.1	1.2	21.6	271.0	19.9	3.4	28.4	1.6
76-17_26	*285.9*	3.2	0.1	0.7	2.6	7.7	14.3	149.0	14.1	9.5	24.4	5.3
76-17_29	*285*	2.5	0.1	1.0	4.1	1.3	21.5	98.0	16.9	3.4	18.2	1.2
76-17_31	*282*	4.0	0.1	1.5	4.1	1.9	30.7	1999.0	22.6	5.3	24.7	1.9
76-17_32	*280*	3.3	0.1	1.1	5.1	1.8	25.1	15.0	13.8	5.1	12.0	1.4
76-17_33	*279.6*	3.6	0.1	1.4	4.1	1.8	26.7	10.0	12.9	4.7	13.9	1.6
76-17_34	*279*	3.7	0.2	1.0	4.3	1.3	21.6	7.0	13.5	4.7	13.9	1.6
76-17_35	*275*	2.9	0.1	5.1	4.1	4.8	86.4	7.0	12.9	3.7	14.0	1.3
76-17_36	*274*	2.7	0.2	0.8	3.9	1.5	15.7	8.0	9.3	4.0	10.6	1.5
76-17_38	*260*	3.8	0.1	0.9	4.1	1.2	16.8	6.0	24.0	4.1	25.9	1.4
76-17_40	*238*	4.7	0.1	2.6	5.4	2.7	53.3	8.0	25.4	8.1	21.1	2.2
76-17_41	*225*	5.1	0.0	0.8	4.3	1.2	29.1	12.0	34.6	4.6	35.9	1.5
median		3.7	0.1	1.0	4.1	1.5	26.6	123.5	18.6	4.7	22.5	1.6
min		2.5	0.0	0.7	2.6	1.1	14.3	6.0	9.3	3.4	10.6	1.2
max		5.1	0.2	5.1	5.4	7.7	86.4	1999.0	34.6	9.5	35.9	5.3
TYK5-1	*155.4*	3.3	0.1	4.3	3.7	4.0	89.9	190.0	14.0	4.6	16.6	1.8
TYK5-2	*155*	5.0	0.1	3.3	5.1	3.1	105.1	86.0	18.9	6.6	16.6	1.9
TYK5-3	*154.18*	5.6	0.1	3.5	4.4	3.1	79.5	25.0	22.8	5.4	23.2	1.8
TYK5-6	*149.08*	3.8	0.1	3.0	4.3	2.7	69.9	15.0	19.5	5.6	20.1	1.9
TYK5-7	*147.54*	2.7	0.1	3.0	4.1	2.8	58.6	8.0	13.7	4.5	15.0	1.6
TYK5-8	*141.29*	3.5	0.1	3.0	4.2	2.8	52.7	11.0	18.4	5.6	19.3	1.9
TYK5-10	*99.41*	2.8	0.1	2.4	3.9	2.4	110.2	258.0	12.9	4.0	14.8	1.5
TYK5-11	*96.37*	2.9	0.1	2.0	4.9	1.8	48.6	1241.0	22.1	5.5	20.2	1.6
TYK5-12	*90.66*	3.0	0.1	2.6	4.2	2.7	64.5	152.0	18.2	4.0	19.0	1.3
TYK5-13	*83.84*	3.2	0.1	1.4	5.4	1.3	44.3	678.0	25.8	5.5	21.2	1.5
TYK5-14	*81.36*	3.0	0.1	1.7	3.3	1.9	50.6	264.0	17.6	3.5	23.5	1.5
TYK5-14A	*80.82*	2.4	0.1	3.1	3.6	3.5	48.8	70.0	14.8	3.6	18.3	1.4
TYK5-15	*77.82*	3.1	0.1	2.7	4.1	2.9	66.3	71.0	18.0	4.5	19.3	1.6
TYK5-16	*76.19*	2.2	0.1	1.7	5.1	1.7	49.2	112.0	17.0	4.8	14.9	1.4
TYK5-17	*73.52*	2.5	0.1	1.4	4.2	1.4	43.2	249.0	14.9	4.2	15.6	1.4
TYK5-18	*72.7*	2.9	0.1	1.2	4.3	1.2	33.9	1751.0	19.2	4.2	20.0	1.4
TYK5-19	*69.81*	2.8	0.1	1.1	4.1	1.2	36.4	692.0	16.9	3.9	18.5	1.4
TYK5-20	*68.72*	2.9	0.1	1.2	4.4	1.2	38.6	2798.0	20.7	4.5	21.1	1.5
TYK5-21	*29.33*	4.2	0.1	1.3	5.9	1.3	54.8	45.0	29.0	5.2	21.7	1.3
median		3.0	0.1	2.4	4.2	2.4	52.7	152.0	18.2	4.5	19.3	1.5
min		2.2	0.1	1.1	3.3	1.2	33.9	8.0	12.9	3.5	14.8	1.3
max		5.6	0.1	4.3	5.9	4.0	110.2	2798.0	29.0	6.6	23.5	1.9
Vent							**wt. %**					
T91.14-11			0.0	5.0	0.6	20.8	0.7	0.0	5.0	1.2		
TYK1-6			0.1	1.9	0.7	26.4	0.0	0.1	3.0	0.7		
TYK2-14			0.0	30.6	0.7	2.0	7.1	0.8	<DL	0.5		
TYK2-15			0.0	8.3	0.5	25.9	9.4	1.9	<DL	0.4		
TYK2-17			<DL	24.7	0.5	17.5	3.8	6.7	<DL	0.3		

Table2

Sample #	Metres	Fe_{mag}	Fe_{ox}	Fe_{carb}	Fe_{py}	Fe_{Hr}	Fe_{py} / Fe_{Hr}	Fe_{Hr} / Fe_T	δ^{98}Mo (‰)				δ^{34}S (‰)
		wt. %							*RochMo2*	*Nist3134*	*2σ*	*n*	
76-17_15	*298*	0.02	0.05	0.55	1.65	2.26	0.73	1.34					-5.7
76-17_17	*292.5*	0.01	0.06	0.16	0.68	0.91	0.74	0.85					-1.4
76-17_18	*292*	<DL	0.04	0.20	0.88	1.12	0.78	0.85	0.79	0.48	0.01	*3*	-1.3
76-17_20	*290*	<DL	0.05	0.34	1.03	1.42	0.72	0.97					-3.5
76-17_22	*287*	<DL	0.04	0.24	1.14	1.42	0.80	0.94					-4.2
76-17_23	*286.8*	<DL	0.03	0.24	0.75	1.01	0.74	0.90					-8.3
76-17_24	*286.5*	<DL	0.04	0.23	0.68	0.95	0.72	0.81	0.88	0.57	0.03	*3*	-4.3
76-17_26	*285.9*	1.38	1.21	3.19	0.50	6.27	0.08	0.81	0.90	0.59	0.02	*3*	-3.2
76-17_29	*285*	<DL	0.07	0.25	0.84	1.17	0.72	0.87	0.84	0.53	0.05	*3*	-0.7
76-17_31	*282*	0.01	0.07	0.45	1.24	1.77	0.70	0.91	0.84	0.53	0.01	*3*	-1.4
76-17_32	*280*	0.02	0.04	0.47	0.85	1.44	0.59	0.80	0.99	0.68	0.01	*3*	-4.1
76-17_33	*279.6*	0.05	0.10	0.26	1.29	1.70	0.76	0.95	1.02	0.71	0.04	*3*	-4.1
76-17_34	*279*	0.03	0.06	0.25	0.66	1.00	0.66	0.77	0.77	0.46	0.03	*3*	-8.6
76-17_35	*275*	0.03	0.14	0.26	3.54	3.98	0.89	0.82	0.79	0.48	0.05	*3*	-13.9
76-17_36	*274*	0.06	0.11	0.50	0.43	1.10	0.39	0.75	0.88	0.57	0.06	*3*	-14.6
76-17_38	*260*	0.03	0.08	0.22	0.69	1.01	0.68	0.86	0.71	0.40	0.05	*3*	-3.6
76-17_40	*238*	0.02	0.06	0.30	2.18	2.55	0.85	0.96					-1.2
76-17_41	*225*	0.02	0.10	0.31	0.60	1.03	0.58	0.87					-15.6
median		0.02	0.06	0.26	0.85	1.29	0.72	0.86	0.84	0.53			-4.1
min		0.01	0.03	0.16	0.43	0.91	0.08	0.75	0.71	0.40			-15.6
max		1.38	1.21	3.19	3.54	6.27	0.89	1.34	1.02	0.71			-0.7
TYK5-1	*155.4*	0.1	0.1	0.4	3.6	4.1	0.87	1.02					8.7
TYK5-2	*155*	0.1	0.1	0.4	2.7	3.2	0.85	1.02	0.80	0.49	0.10	*4*	6.9
TYK5-3	*154.18*	0.0	0.1	0.3	2.6	3.0	0.87	0.95	1.00	0.69	0.02	*3*	6.5
TYK5-6	*149.08*	0.0	0.1	0.3	2.6	2.9	0.88	1.06	0.84	0.53	0.05	*3*	3.1
TYK5-7	*147.54*	0.0	0.1	0.3	2.4	2.8	0.87	0.99	0.67	0.36	0.05	*3*	6.5
TYK5-8	*141.29*	0.0	0.1	0.2	2.5	2.8	0.89	1.01	0.73	0.42	0.03	*3*	4.3
TYK5-10	*99.41*	0.0	0.1	0.3	2.0	2.3	0.85	0.96	0.81	0.50	0.09	*4*	8.1
TYK5-11	*96.37*	0.0	0.0	0.2	1.4	1.7	0.84	0.95	0.66	0.35	0.06	*3*	1.7
TYK5-12	*90.66*	0.0	0.1	0.5	2.0	2.6	0.79	0.96	0.82	0.51	0.04	*3*	-1.2
TYK5-13	*83.84*	0.0	0.0	0.1	1.1	1.3	0.85	0.97	0.66	0.35	0.11	*3*	-4.4
TYK5-14	*81.36*	0.0	0.1	0.4	1.4	1.9	0.74	1.02	0.75	0.44	0.07	*5*	3.2
TYK5-14A	*80.82*	0.0	0.0	0.7	2.7	3.5	0.78	0.99	0.89	0.58	0.03	*3*	8.3
TYK5-15	*77.82*	0.0	0.0	0.6	2.7	3.4	0.81	1.16					7.8
TYK5-16	*76.19*	0.0	0.0	0.2	1.4	1.7	0.82	0.98					-0.3
TYK5-17	*73.52*	0.0	0.0	0.1	1.4	1.6	0.86	1.17					1.7
TYK5-18	*72.7*	0.0	0.0	0.2	0.9	1.2	0.78	0.93					-0.8
TYK5-19	*69.81*	0.0	0.0	0.2	0.9	1.1	0.79	0.92					-0.7
TYK5-20	*68.72*	0.0	0.0	0.1	0.9	1.1	0.85	0.93	0.70	0.39	0.08	*4*	-0.5
TYK5-21	*29.33*	0.0	0.0	0.2	0.8	1.0	0.78	0.73					-5.3
median		0.02	0.05	0.26	1.96	2.31	0.85	0.98	0.78	0.46			3.09
min		0.01	0.03	0.13	0.75	0.96	0.74	0.73	0.66	0.35			-5.27
max		0.10	0.07	0.71	3.59	4.11	0.89	1.17	1.00	0.69			8.71
SDO-1									1.11	0.80	0.06	*11*	
KyotoMo									-0.06	-0.37	0.04	*11*	
ImperialMo									0.15	-0.16	0.05	*10*	